ISSN 1069-3513, Izvestiya, Physics of the Solid Earth, 2010, Vol. 46, No. 2, pp. 104–135. © Pleiades Publishing, Ltd., 2010.
Original Russian Text © V.B. Smirnov, A.V. Ponomarev, P. Benard, A.V. Patonin, 2010, published in Fizika Zemli, 2010, No. 2, pp. 17–49.

Regularities in Transient Modes in the Seismic Process according to the Laboratory and Natural Modeling

V. B. Smirnov[a, b], A. V. Ponomarev[a], P. Benard[c], and A. V. Patonin[d]

[a] *Schmidt Institute of Physics of the Earth, Russian Academy of Sciences, ul. Bol'shaya Gruzinskaya 10, Moscow, 123995 Russia*

[b] *Faculty of Physics, Moscow State University, Moscow, Russia*

[c] *Institute de Physique du Globe de Paris, Paris, France*

[d] *Borok Geophysical Observatory, Schmidt Institute of Physics of the Earth, Russian Academy of Sciences, Borok, Nekouz, Yaroslavl' region, 152742 Russia*

Received September 21, 2009

Abstract—Regularities in the excitation and relaxation of rock failure were revealed in a series of laboratory experiments. Similar regularities are found also in natural conditions. A physical idea and its mathematical description are suggested for explaining the obtained experimental data. The aim of the experiments was to understand the character of excitation of the failure, triggered by the external impact, and its relaxation after the cessation of the pressure, depending on the intensity of the acting stresses. Different rates of increase in the initiating strains result in different acoustic responses that reflect the development of failure. At the higher rates of deformation, the observed process was similar to the aftershock sequences, and at the lower, to the seismic swarms. The character and parameters of the acoustic response change with the increase in the acting strains. The patterns of the changes exhibit several regularities. In case of the swarm-like activity, the time of maximum activity (and, correspondingly, the beginning in its decay) increases with the increase in acting strains. In case of the aftershock-like activity, the level of applied strains determines the parameters of the Omori's law. The delay in the power-law's decrease in activity increases with the growth of the load (similar to the increasing time until the beginning of the decay in the swarm-like activity). Similar regularities are defined in natural conditions in the experiments on the rock's failure induced by water infusion into a borehole (Soultz-sous-Forêts, France). A hypothesis of competitive excitation and relaxation is suggested for explaining the observed experimental data. Mathematical modeling has confirmed the validity of this hypothesis.

DOI: 10.1134/S1069351310020023

Numerous works addressing the analysis of the seismic regime highlighted several challenging problems, one of which is connected with insufficient knowledge of physics of transient modes, reflecting the general dynamics of seismicity arising in response to different exciting factors. The seismic process involves different-type feedbacks that determine and control the evolution of seismicity. It is difficult to reveal and study these feedbacks in stationary conditions, since the variations in the background seismicity are insignificant, and their nature is usually poorly known. The transient mode of the seismic process is a response of the geophysical medium to the different impacts that disturb its stationary state. Identification of the regularities in the transient mode offers the possibility to gain an insight into the character and specific features of the key properties of the medium and its physical mechanisms, which govern the dynamics of the seismicity.

The study of transient modes provides methodological advantages, since it draws together the geophysical study in free natural conditions and the laboratory physical experiment with controlled conditions and repeatability of tests. Regarding the study of the transient seismic regimes, we have a priori knowledge about the exciting source and may assess the repeatability of natural experiments.

The dynamical model describing the nucleation of the sources of real earthquakes may be represented as the initiation and development of macrofractures in the laboratory experiments, which provides the grounds for subsequent modeling of the seismic regime. Such experiments are successfully carried out by several research teams [Yanagidani et al., 1985; Lockner et al., 1992; Yukutake, 1992; Lei et al., 1992; 2000; Lockner, 1993; Moore and Lockner, 1995; Zang et al., 2000; Thompson, 2006; Fortin, 2006].

The purpose of our experiments was to study the character of rock the failure initiated by an external impact and its relaxation after the cessation of the impact, and to find the correlation between these processes and acting stresses. The experiments were conducted in the Borok Geophysical Observatory of the Institute of Physics of the Earth, Russian Academy of Sciences. We also took into consideration the data, obtained in the unique experiments on the crushing of large blocks of rocks at the high-pressure press in the

Institute for High Pressure Physics (Russian Academy of Sciences) [Semerchan et al., 1981; Sobolev and Kol'tsov, 1988] and in a natural experiment at the European test site in Soultz-sous-Forêts [Cornet et al.; 1977; Evans et al., 2005a; 2005b; 2005c; Gerard et al., 2006]. The experimental results are illustrated by the mathematical model.

EXPERIMENTAL TECHNIQUE AND METHODS

The studies were conducted with the uniaxial load of the specimen, including the experiments with uniform compression. The typical sizes of the sandstone and limestone specimen varied from a few centimeters to 1 m. The parameters of the specimen and the regimes of the initiation of the rock failure are given in the table. The names of the experiments discussed in the text correspond to the names of the specimen. The velocities of the elastic waves cited in the table were measured prior to the experiments; the open porosity was determined by the method of water saturation in the vacuum chamber.

The first series of the experiments was performed at the programmable geophysical complex with the two-chamber electrohydraulic press INOVA-1000. The maximal load provided by this system is 1000 kH, the maximal stroke of the mobile hob is 100 mm, and the working zone is 300 × 300 × 800 mm in size. The control system is implemented as a programmable feedback controller; the accuracy of the load control is up to 5 N; the piston stroke control accuracy is ±0.05μm; and the strain-control accuracy is <0.17 μm. The piston stroke is executed in discrete steps with minimum increment of 0.24 μm. The control program provides the following modes of operation: loading with the constant rate of strain and its possible variations during the experiment, the standby mode (retention of the constant strain), additional harmonic modulation of the axial pressure, and checking the loading rate under the acoustic emission (AE) feedback. The axial load, piston stroke, and other mechanical parameters were measured at the sampling rate of 1 s.

A uniform compression of up to 200 MPa is provided by the oil pressure in the high-pressure chamber. Cylindrical specimen of sandstone, 30 mm in diameter and 60 mm long are mounted in a special measurement cell equipped with sensors of the axial load and radial deformation, and with piezoelectric receivers of the acoustic signals. During the measurements, the samples are sealed by copper and plastic jackets.

The acoustic emission (AE) signals are measured using two independent recording systems. The first system is a multichannel station for recording the waveforms. The incoming AE signals are received by eight resonance (375 kHz) piezoelectric receivers, then amplified by preliminary amplifiers, and digitized with a 5 MHz sampling frequency.

During the process of loading, the ultrasonic sounding of the specimen is carried out from several directions for calculating the velocities of elastic waves used for calculation of the coordinates of acoustic pulses. Errors in the identification of the first arrivals of the elastic waves do not exceed fractions of microseconds, which results in the errors of coordinates not higher than 1.0–1.5 mm. In the method for calculation of the coordinates, an iteration procedure is used for minimization of the misfits between the calculated data and the arrival times derived from instrumental measurements.

The system for recording the waveform has several constraints caused by the discontinuous contact of the sensors with the specimen; therefore, the energy of the recorded signals and the number of localized events may not always be correctly estimated. More accurate assessment of these parameters may be yielded by a one-channel system of continuous recording of the acoustic signals. Such an approach is implemented in recent studies to eliminate the constraints related to the trigger (threshold) method of signal detection [Thomson et al., 2006]. In this system, a piezoelectric sensor with the resonance frequency of 290 kHz mounted in the lower piston of the press is used as a receiver. The acoustic contact of the sensor with the specimen is provided by the axial load itself. This yields a reliable and stable acoustic contact with the lower part of the specimen during the entire experiment, including the terminal stage of the rock failure. The amplified signal is continuously sampled at 1 MHz. The preliminary processing of the data includes their aggregation and calculation of the effective amplitude over the interval of 96 μs.

The subsequent processing aimed at the extraction of the separate acoustic emission signals is based on the automatic adaptive detection of signals in accordance with the threshold criterion. The system allows the flow of signals to be processed at a rate of 2400 events per second. The processed data are compiled into the catalog of events, which includes the time of the event and its energy. Precisely these data are analyzed in this work.

The steps of strain with different rates of increase and different duration were used as a triggering impact. Two different regimes of the uniaxial load were applied.

The first regime is the step under a maximally rapid single stroke of the hob and the subsequent retention of the specimen under constant strain conditions. (Hereinafter, we will refer to this regime as "a sharp step.") The strain rate defined by the technical characteristics of the press was in this case at least 10^{-3} l/s. As was shown earlier [Smirnov and Ponomarev, 2004], the small sharp stepped growth in the load applied to the specimen induces acoustic activity similar in its statistical properties to the aftershock sequences: the acoustic activity obeyed Omori's law, and the observed temporal changes in the acoustic parameters were similar to those characteristic of the aftershocks. After the acoustic activity had returned to its background level (this occurred usually after 200–400 s), the additional stepped loading was repeated.

The second regime was characterized by the linear increase of the strain with the rate specified in the interval of approximately 10^{-6} to 10^{-5} l/s. This increase was followed by keeping the specimen under constant deforma-

Characteristics of specimen and the modes of initiation

Parameters of the specimen							Characteristic of the initiation				Catalogue
Specimen	Material	Size, mm	Density, g/cm^3	Porosity, %	P-wave velocity, km/s	S-wave velocity, km/s	Rate of increase in the step of deformation or stress	The value of the step of strain or stress step	Duration of intervals of the load increase/retention	Uniform compression, MPa	Total number of events
A42	Sandstone	∅ 30, length 60	2.16	14.6	2.20	1.78	at least 3×10^{-3} 1/s	3.25×10^{-4}	(not more than 0.1)/1250 s	None	115085
A52			2.14	14.6	2.32	1.75	2.0×10^{-5} 1/s	4.07×10^{-4}	20/(80–460) s	None	246207
A62			2.51	4.5	4.37	2.87	2.0×10^{-6} 1/s	4.07×10^{-4}	200/400 s	None	438355
SS40			2.24	21.3	2.54	1.59	4.0×10^{-6} 1/s	8.14×10^{-4}	200/400 s	40	2548533
SS70			2.25	21.9	2.59	1.71	4.0×10^{-6} 1/s	8.14×10^{-4}	200/400 s	70	5202922
LL1	Limestone	1000 × 500 × 500	2.3	7	3.8	2.5	1.1×10^3 Pa/s (1.4×10^{-7} 1/s)	2 MPa (2.5×10^{-4})	30/30 min	None	20400

Note: Petrographic characteristics of specimen. (A42, A52) sandstone, polymictic, light, inequigranular. The grain size varies from 50 to 300 μm. The main characteristic of the mineral composition: high content of clay minerals and carbonates (calcite and dolomite). Composition: quartz 30–35%, feldspar 30–35%, biotite up to 10%, cementing material (clay minerals, carbonates) up to 15%, ore minerals and oxides up to 5%.
(A62) sandstone, arkosic, fine-grained, brown. The average grain size is 150 μm. The main characteristic of the mineral composition: low content of clay material. Composition: quartz 75%, feldspar 15%, cementing material (clay minerals, oxides, carbonates) up to 5%, ore minerals and their oxides up to 5%.
(SS40, SS70) sandstone, arkosic, transitional to feldspar–quartzose. The grain size is 300–400 μm. The mineral composition: quartz 65%, feldspars 25%, cementing material (clay minerals, carbonates) 10%, rare mineral phases
(LL1) shell limestone. Mineral composition: calcite 50%, dolomite 30%, clayey material filling fractures 20%. Values and growth rates of deformations are different for different series; in brackets: average values.

tion and subsequent continued loading in line with the same procedure. Let us term this regime of initiation as a smooth step.

Some experiments were conducted under uniform compression at 40 and 70 MPa.

The strain control regime was selected in accordance with the notion about the processes occurring in the focal zones of earthquakes. In the context of earthquake focal mechanics, the source of an earthquake is modeled at first approximation by the step-like source time function [Kostrov and Das, 1988], which is the key factor determining the further evolution of the stress-strain state of the medium and the process of fracturing that manifests itself in the natural conditions as the aftershock sequences .

The acoustic catalogues that were compiled from the data obtained in the experiments included tens to hundreds of thousands of events. Preprocessing of the catalogue data was carried out in accordance with the technique applied previously in similar experiments for assessing the uniformity of the data from different seismic catalogues [Smirnov et al., 1995; Smirnov, 1997]. The amplitude of the acoustic impulses was recalculated into the conditional energy class by the formula $K = 2\log A$, , where A is the averaged amplitude of the electric signal coming from the acoustic sensor (no absolute calibration of the mechanical–electrical converter was carried out). Assuming an insignificant difference between the pulse spectra and continuous contact of the sensor with the specimen, A^2 is proportional to the seismic energy, and K in this case is similar in its physical meaning to the energy class applied in seismology.

We also again analyzed the data obtained in previous experiments on fracturing the large (approximately 1 m^3) rock blocks [Sobolev et al., 1996]. Such experiments are of particular significance, since they allow for the study of the local internal failure, with the exclusion, or diminished influence, of the external boundaries of the blocks and with decreasing the effect of the crushing of the specimen by the loading unit. Due to the natural heterogeneity of large blocks, some volumes inside the specimen that are surrounded by the harder material may be crushed, which is likely characteristic of earthquakes. These experiments make it possible also to estimate the influence of the scaling factor on the failure and to compare the results of the laboratory experiment with the natural patterns.

UNIAXIAL LOADING WITHOUT UNIFORM COMPRESSION (SMOOTH STEP)

Figure 1 illustrates the loading history of the sandstone specimen (A52) with its initiation by the smooth step. Each load step induced a burst of acoustic activity. During the retention periods of the specimen, a gradual decay was observed in the axial strain; moreover, the higher the acoustic activity, the larger the decay at each step of loading.

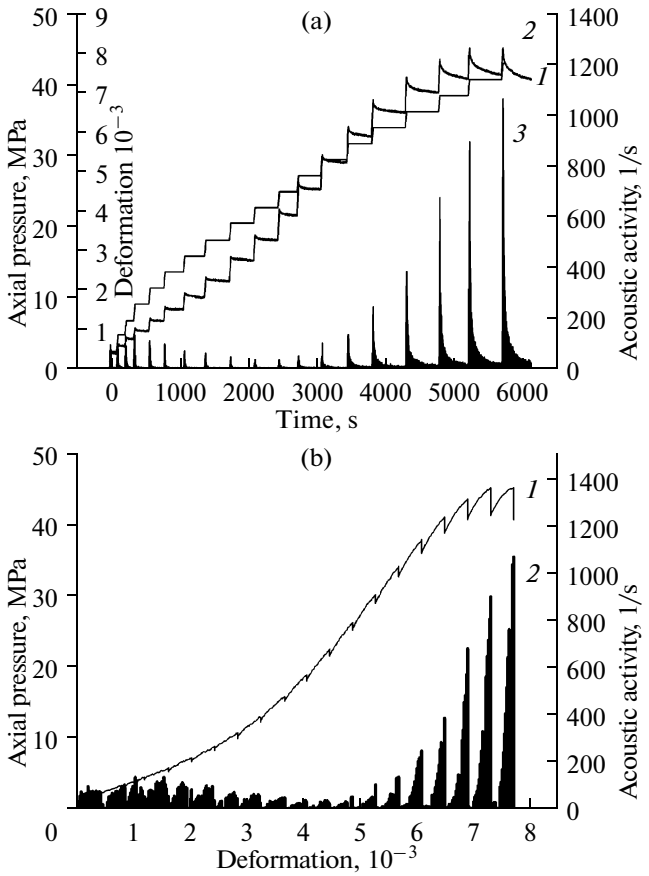

Fig. 1. Loading history and loading curve for Specimen A52: (a) loading history: (*1*) axial stress, (*2*) axial strain, (*3*) acoustic activity; (b) loading curve: (1) stress–strain diagram, (*2*) acoustic activity.

The curve of loading presented in Fig. 1b is typical for the experiments without uniform compression when the stresses are applied by the press only to the end faces of the cylindrical specimen, while its lateral faces are free of load (let us name this regime as a purely uniaxial load). Direct measurements show that highly porous substances experience significant inelastic deformations even under low stresses [Hart and Wang, 1995; Lockner and Stanchits, 2002]. Figure 1b clearly demonstrates the nonlinear correlation between the stresses and deformations in the initial part of the load curve. This interval corresponds to relatively high acoustic activity, which decreases with the increase in the stresses and reaches its minimum as the load curve passes to the straight-line segment.

The smoothing of the initial part of the load curve in the experiments with the purely uniaxial loading (particularly in case of a porous medium) is usually explained by the closure of pores and fractures as well as by the "settling-down" of mineral grains [Scholz, 1968; Tapponnier and Brace, 1976; Lavrov et al., 2004; Paterson and Wong, 2005]. This process is accompanied by acoustic activity.

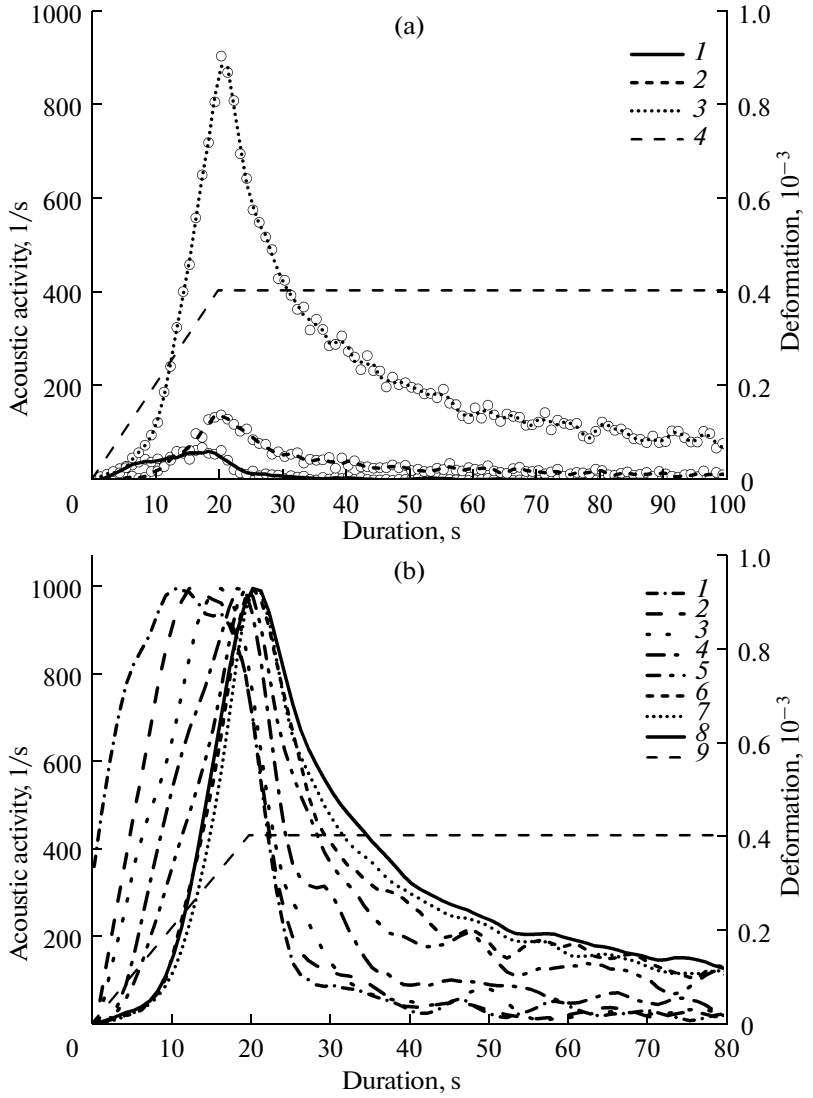

Fig. 2. Acoustic activity in the experiment A52: (a) examples of initial data (points) and smoothed curves corresponding to different values of acting stresses: (*1*) 8.3 MPa, (*2*) 29.2 MPa, (*3*) 41.3 MPa, (*4*) initiating step of deformation; (b) normalized curves of acoustic activity under different acting stresses: (*1*) 1.0 MPa, (*2*) 5.3 MPa, (*3*) 10.2 MPa, (*4*) 15.3 MPa, (*5*) 21.7 MPa, (*6*) 29.2 MPa, (*7*) 39.2 MPa, (*8*) 42.1 MPa, (*9*) initiating step of deformation.

The material weakened by the preexisting defects is characterized by lowered effective elasticity modules, which is reflected in the smoothing of the load curve. With the exhausting of the existing defects, the closing of the pores and microfractures, the rigidity of the mineral matrix and, correspondingly, the effective increase of the elasticity modules, the load curve passes to a straight-line interval [Hart and Wang, 1995].

Let "a series" be the term denoting the period of the experiment that begins at the first point of the growth in the step of initiating deformation and ends at the last point of the area with constant deformation. Let the level of acting stress (or simply, the acting stress) be understood as the stress (axial pressure), which was the starting value in the initiation by the step-like strain of a given series (due to the fact that the strains vary within a series, we used the average value for the series preceding the one under consideration). In the representation of the results for the individual series, the time is always counted from the beginning of the series.

Figure 2a presents examples of several series, corresponding to different levels of acting strains. It is seen that the load steps induced acoustic activity resembling seismic swarms: with the gradual growth and subsequent decay in the activity. The intensity of the acoustic activity in different series is characterized by different statistical scatter explained by the different volumes of the data sets analyzed: at higher strains, the curves are calculated using a greater amount of events. Therefore, the initial data were smoothed by their averaging in the corresponding sliding windows, and only smoothed data were used in the further analysis.

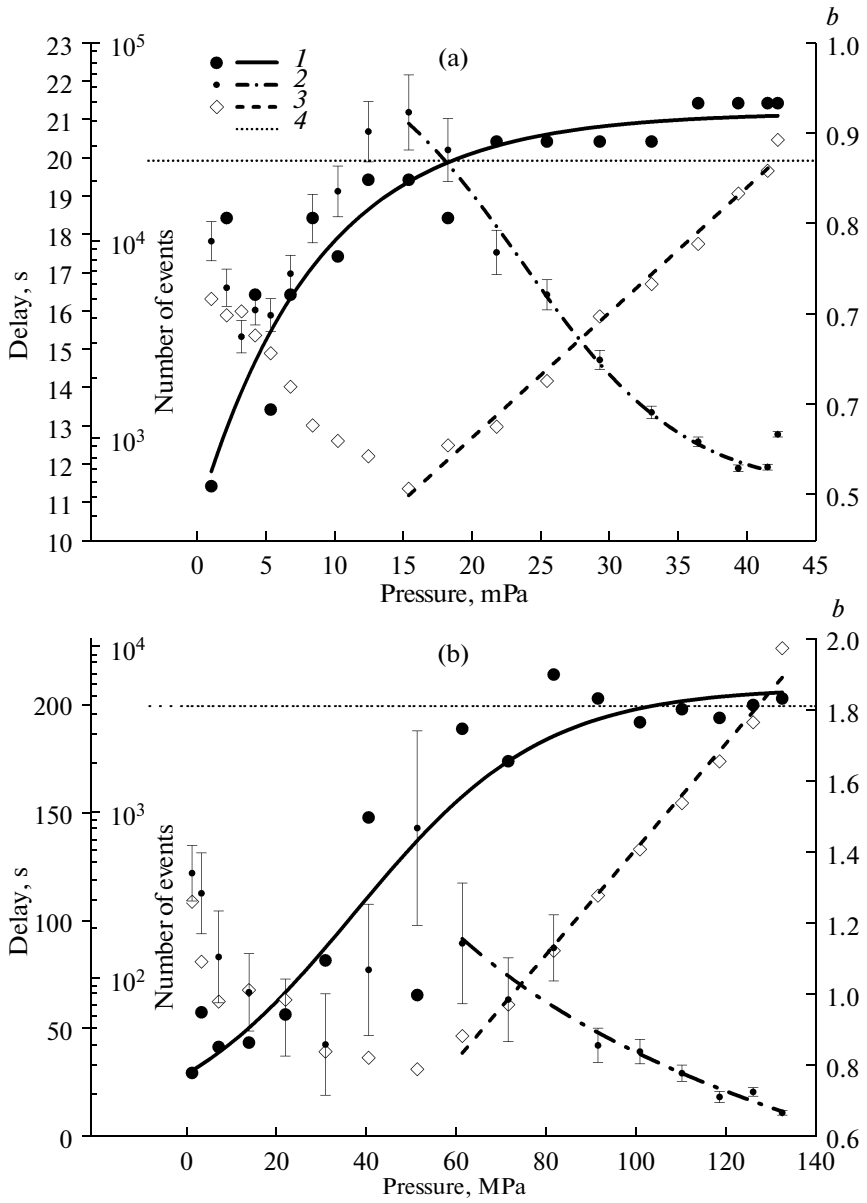

Fig. 3. Parameters of the acoustic regime with different acting stresses: (a) experiment A52, (b) experiment A62: (*1*) delay in maximum activity relative to the beginning of initiation, (*2*) slope of the frequency-magnitude curve, (*3*) number of events in each series (the straight line corresponds to exponential approximation), (*4*) the duration of the increase of the initiating step: 20 s in A52 and 200 s in A62.

It is apparent in Fig. 2a, that under high strains, the maximum activity shifts to higher time values. For the purposes of better visualization, the activity in each series was normalized to its maximum. The results are shown in Figure 2b (only several series are presented for easier readability of the image). One can see that the time shift (delay) of the maximum activity relative to the start of the initiation (beginning of the series) increases with the increase in the acting stresses. It is noteworthy that at low strains the maximum falls into the interval of the buildup in the step load; i.e., the decay in the acoustic activity begins and proceeds under an increasing initiating load.

Figure 2a depicts also the delay of the maximum activity (the beginning of the decay in the activity, the beginning of the relaxation of excitation) depending on the acting stresses. The increase in the delay of the maximum activity (and, correspondingly, the increase in the delay of the start in relaxation of the perturbation) depending on the acting stresses is apparent. It is seen also that at high stresses the activity continues to grow even after the growth in the initiating step has stopped: the delay of the maximum activity exceeds the duration of the period of increasing stresses.

Figure 3a also displays the complete set of the acoustic events recorded in each series. The slope of the curve of

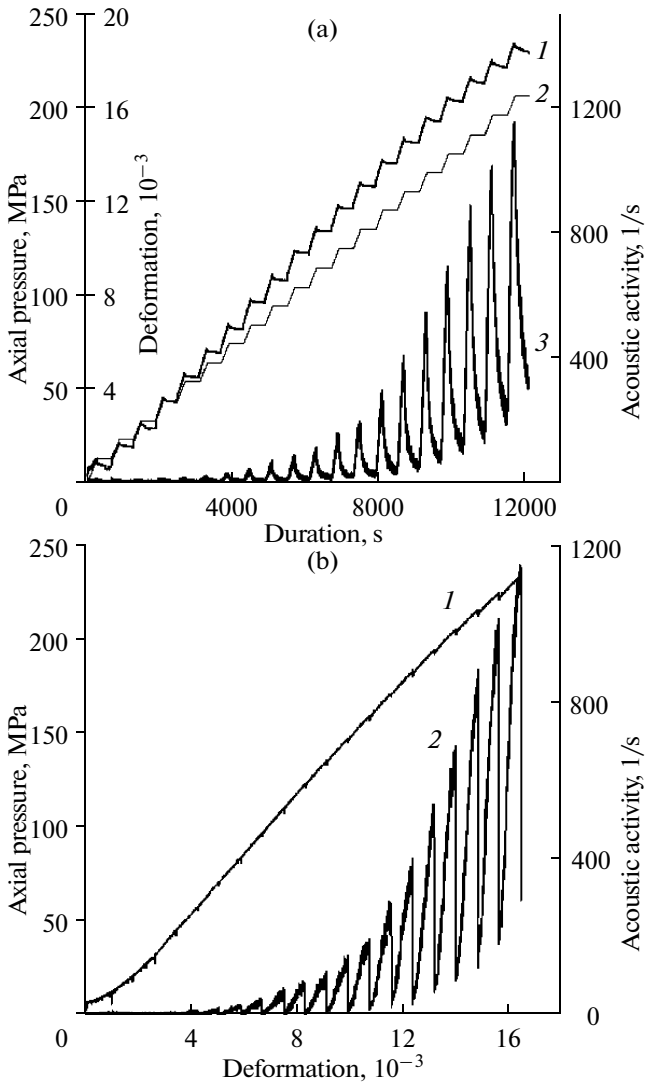

Fig. 4. Loading history and loading curve for Specimen SS70: (a) loading history: (*1*) axial stress, (*2*) axial deformation, (*3*) acoustic activity; (b) loading curve: (*1*) stress–strain diagram, (*2*) acoustic activity.

the frequency-magnitude relation estimated from the whole set of these events is also presented. The slope of the magnitude-frequency plot is estimated using the method of maximal likelihood accepted in seismology, taking into account the representativeness of the catalogues of the acoustic events. The correlation between these parameters and the acting stresses is typical in the experiments with purely uniaxial loading.

As mentioned above, the acoustic activity at the initial stage of loading is evidently associated with the failure of the preexisting defects. In Fig. 3a, this stage corresponds to the descending branch of the curve depicting the number of events. It is seen that at the failure of preexisting defects and the transition of the load curve to its straight-line segment (Fig. 1), the slope of the plotted frequency-magnitude relation increases. Consequently, as the stresses increase, the portion of progressively smaller defects among the failed defects increases. This is consistent with the notions on the correlation between the strength of preexisting defects and their size: the larger the defect, the lower its strength (the classical example of this phenomenon is represented by Griffith's fracture). In the beginning, the lower loads result in the fracturing of the largest (and, correspondingly, the least failure-proof) defects. With the enhancement of the load, the stresses become sufficient for causing the failure of smaller (and, thus, stronger) defects.

Further increase in the load results in the formation of new fractures, and the failure develops in line with the kinetic concept by [Zhurkov, 1968] and the avalanche–unstable fracturing scenario [Mjachkin et al., 1975a; 1975b]. This is confirmed by the exponential dependence of the number of events on the stress value and by the decrease in the slope of the frequency-magnitude plot typical for the processes of the crack fusion and growth [Zhurkov et al., 1980; Sobolev, 1993; Reches and Lockner, 1994; Xinglin Lei et al., 2003].[1]

In Fig. 3a, we drew a single smooth line through the points of the dependence of the delay in the maximum activity relative to the beginning of the initiation. Each phase of the failure (of both preexisting defects and newly formed fractures) should perhaps be considered separately, and different approximations should be perhaps constructed for the delay. Which of these approaches is more valid remains unclear so far; the answer to this question requires special studies.

Figure 3b displays the dependences of the delays of maximum activity, the amount of the acoustic events, and the slope of the frequency-magnitude curve on the acting stresses for experiment A62. In the material of the specimen and load regime, this experiment is similar to the previous one (A52), although the strength of Specimen A52 proved three times higher than that of Sample A62. It is apparent that the results of this experiment are also similar to those shown in Fig. 3a: the delay grows with increasing stresses, the slope of the frequency-magnitude curve decreases, and the number of events is approximated by the exponential dependence (beyond the interval corresponding to the failure of the preexisting defects).

NIAXIAL LOAD UNDER UNIFORM COMPRESSION (SMOOTH STEP)

The loading history and the load curve with initiation by the smooth step under uniaxial loading and uniform compression (experiment SS70) are presented in Fig. 4. The uniform compression allows significant suppressing

[1] Zhurkov's formula proposed for material durability is in essence the Boltzmann exponent. The value reciprocal to the durability determines the probability of failure; therefore, in the context of the kinetic concept, the exponential dependence of the number of failure events during a certain period on the applied stresses should be expected [Regel et al., 1974].

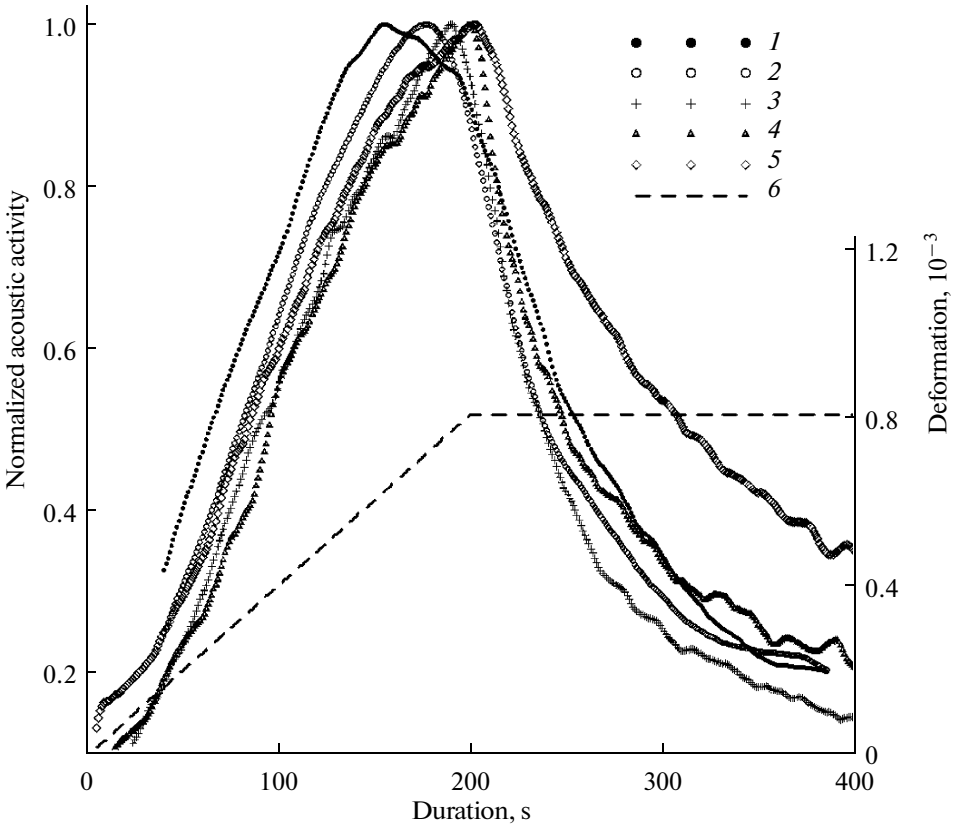

Fig. 5. Normalized curves of acoustic activity under different acting differential stresses and the initiating step of deformation (experiment SS70): (*1*) 30 MPa, (*2*) 55 MPa, (*3*) 105 MPa, (*4*) 155 MPa, (*5*) 215 MPa, (*6*) initiating step of deformation.

of the role of the failure of preexisting defects [Zhang et al., 199; Kawakata and Shimata, 2000; DiGiovanni et al., 2000]. It follows from Fig. 4 that the above-mentioned effects of smoothing of the load curve and the decrease in the acoustic activity at the initial stage of the load can be observed only in the situation when the axial load additional to the uniform compression (which is named the "differential") is lower than the hydrostatic pressure that provides the uniform compression. With the differential load exceeding the hydrostatic pressure, the effects of the failure of preexisting defects may be disregarded. In addition, the uniform compression increases the strength of the specimen, thus allowing the experiments to be carried out with a higher axial load, which yields, correspondingly, more extensive acoustic catalogues.

Figure 5 presents the normalized curves of the acoustic activity for the initiation series with different acting differential stresses (only several series are shown). It is clearly seen that the delay in the maximum activity increases with the increasing stresses.

The results of the experiments on the initiation under the uniform compression are summarized in Fig. 6. The regularities observed in the variations of the parameters are the same as in the case of the purely uniaxial load: with the growth in the acting stresses, the time interval to the commencement of relaxation (to the beginning of the decay in the activity) increases, and the slope of the frequency-magnitude plot decreases. The dependence of the total amount of events in each series on the stress is close to the exponential one.

The catalogues of the acoustic events observed in the experiments with uniform compression are sufficiently extensive to provide the possibility for studying the temporal variations in the slope of the frequency-magnitude curve within each series. It is possible to obtain the representative estimates for the "major" series, i.e., under relatively high acting stresses and, correspondingly, high acoustic activity. Figure 7, which presents such estimates, shows the regular variations in the slope of the frequency-magnitude curve (b): at the stage of increasing acoustic activity b decreases, while at the stage of a reduction in activity, it increases. The higher the level of acting stresses (i.e., the closer the material is to the critical state characterized by failure emergence), the stronger is the effect (variations in b are stronger).

The experiments with a purely uniaxial load (without uniform compression) reveal the same trend in the changes of the slope of the frequency-magnitude curve, although the insufficient data set prevented us from obtaining the statistically reliable estimates; therefore, we omit the corresponding plots here.

The decrease in the slope of the frequency-magnitude curve with time is also known to be observed during the

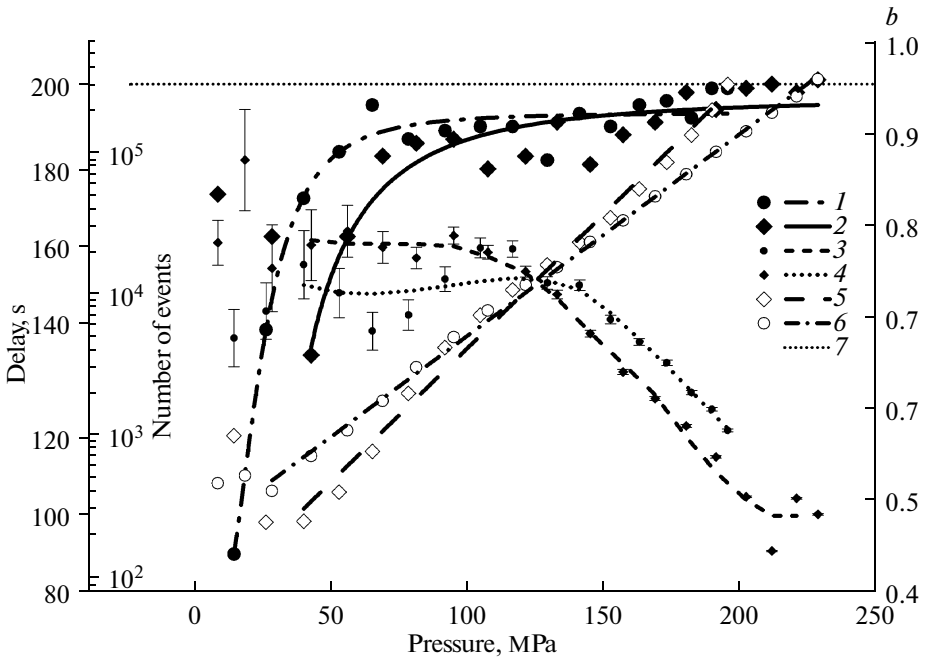

Fig. 6. Parameters of the acoustic regime with different acting differential stresses (experiments SS40 and SS70): (*1, 2*) delay in maximum activity relative to the beginning of initiation (SS40 and SS70, respectively), (*3, 4*) the slope of the frequency-magnitude curve (SS40 and SS70, respectively), (*5*, 6) number of events in each series (SS40 and SS70, respectively), the straight lines correspond to exponential approximations), (*7*) duration of the interval of the increase in the initiating step: 200 s.

preparation of an earthquake [Zhang and Fu, 1981; Smith, 1981; Main et al., 1989; Meredith et al., 1990; Zav'yalov, 2006]. This phenomenon is believed to be related to the gradual redistribution of the process of fracturing in scales, which develops from lower to higher scales (the crack instability avalanche model) [Sobolev, 1993]. The increase in b is typical during the relaxation of the seismic activity in the aftershock sequences. It indicates that the relaxation is accompanied by both a decrease in the seismic activity and the scale redistribution of the failure processes. In [Smirnov and Ponomarev, 2004] it is shown that immediately after the main event the failure processes are focused mainly on large-scale events, whereas during the relaxation it involves smaller events, eventually degrading to the uniform redistribution, which is characteristic of the background seismic activity. The data shown in Fig. 7 indicate that in case of the swarm-like activation without a pronounced main event, the excitation and relaxation probably develop in accordance with the same scenarios.

UNIAXIAL LOAD (SHARP STEP)

Figure 8 displays the history of loading of Sample A42 with excitation by a sharp step. The load curve (Fig. 8a) is typical for the experiments without uniform compression.

Figure 9a presents the examples illustrating the changes in the acoustic activity $\dot{n}$ for several series. The changes in $\dot{n}$ are similar to the aftershock sequences; in Fig. 9a, the $\dot{n}$ value is approximated in accordance with the modified Omori's law:

$$\dot{n} = \frac{\dot{n}_0}{(t+a)^p}. \quad (1)$$

Figure 9a demonstrates the summary of approximations (1) for all series. It is seen that the time delay of the beginning of the power-law relaxation increases with the increase in the series number and, correspondingly, with the increase in the acting stresses (note that the reason for the anomaly in the 5th series is unknown). The similar "shelf" at the beginning of the activity decay is known also for the aftershock sequences [Smirnov and Ponomarev, 2004]. Its nature is not quite clear so far. Some authors explain it by the refractoriness of the seismic network (the overload of the network by too many earthquakes and, correspondingly, the omission of some of them). However, physical explanations for the delay in the beginning of the power-law relaxation of the aftershock activity are available [Narteau et al., 2002]. In the works [Smirnov and Lyusina, 1990; Lyusina and Smirnov, 1993; Marsan and Bean, 2003], it is noted that the initial stage of aftershocks, occurring within a few days after the main event, differs from the subsequent one not only in the anomalously slow extinction of the activity but also in the patterns of the temporal and spatial–temporal clustering of the events.

Figure 10 illustrates the variations in the parameters a and p of the modified Omori's law (1), depending on the

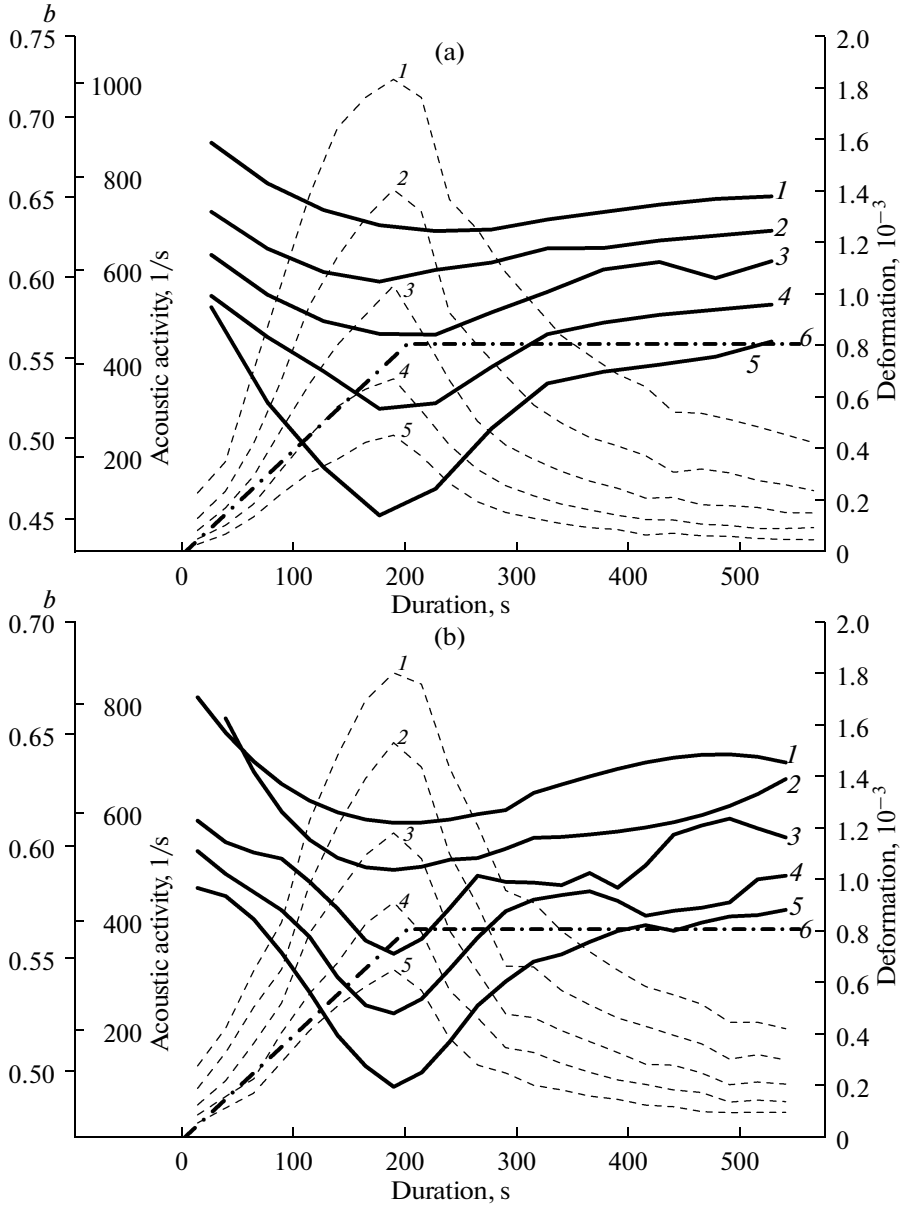

Fig. 7. The slope of the frequency-magnitude curve in the series: (a) experiment SS40: (*1*) 140 MPa, (2) 152 MPa, (*3*) 163 MPa, (*4*) 173 MPa, (*5*) 182 MPa, (b) experiment SS70: (*1*) 180 MPa, (*2*) 191 MPa, (*3*) 202 MPa, (*4*) 211 MPa, (*5*) 220 MPa. The dashed line indicates corresponding curves of acoustic activity. (*6*) initiating step of deformation.

acting stresses. It is seen that the both parameters increase with the increasing stresses.

Figure 10 presents also the number of the acoustic events in each series. At the prepeak stage of load, the dependence of the number of events on the stresses is close to the exponential one, which is consistent with the kinetic concept of the failure. At the postpeak stage, when the growth in strains is accompanied by the decrease in stresses (Fig. 8), the acoustic activity continues increasing (the corresponding points in Fig. 10 lie above the straight line). In terms of the kinetic concept, this can be explained either by the growth in the Zhurkov's structurally–sensitive parameter at the postpeak stage, due to the sharp increase in the fracturing of the medium or by the decrease in the effective section of the specimen caused by the same reason and, correspondingly, the increase in the local stresses.

Thus, the initiation by the sharp step results in the excitation of the aftershock-like acoustic activity. The magnitude of the activity and the parameters of the Omori's law depend on the intensity of the stresses acting during the initiation. The higher the acting strains, the later the power-law relaxation typical of aftershocks begins.

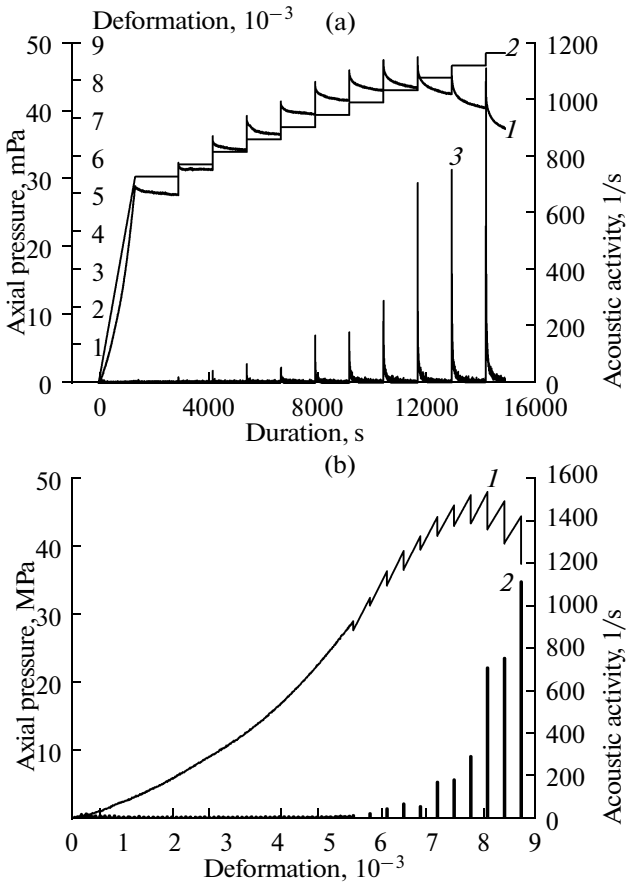

Fig. 8. Loading history and loading curve for Sample A42: (a) loading history: (*1*) axial stress, (*2*) axial deformation, (*3*) acoustic activity; (b) loading curve: (*1*) stress–strain diagram, (*2*) acoustic activity.

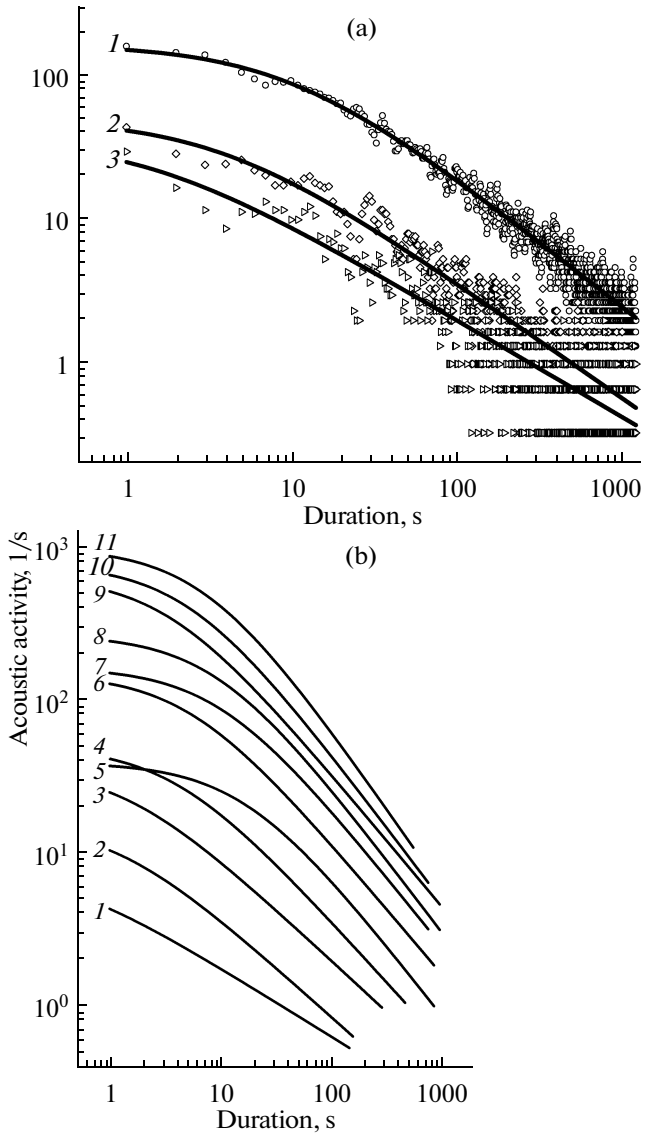

Fig. 9. Acoustic activity in experiment A42: (a) examples of initial data (points) and approximation by the Omori's law $\dot{n} = \dfrac{\dot{n}_0}{(t+a)^p}$ under different acting strains: (*1*) 31.4 MPa, (*2*) 34.4 MPa, (*3*) 41.2 MPa, (b) summarized Omori's law approximations for all series: (*1*) 27.5 MPa, (*2*) 27.9 MPa, (*3*) 31.4 MPa, (*4*) 34.4 MPa, (*5*) 36.8 MPa, (*6*) 39.7 MPa, (*7*) 41.8 MPa, (*8*) 43.4 MPa, (*9*) 43.9 MPa, (*10*) 43.2 MPa, (*11*) 41.2 MPa.

LARGE-SCALE LABORATORY MODELING

The laboratory experiments on the initiation of failure were carried out on another scale as well. These works were conducted using the high-pressure press in the Institute of Physics of High Pressures (Russian Academy of Sciences) in 1993. The parameters of the acoustic emission were studied during the stepped load of a large block of shell limestone. The sample LL1 was essentially heterogeneous with cavities up to 1 cm across and fractures up to a few centimeters long.

The block was loaded along the long face by the uniaxial stress. Each loading series lasted 1 h and included two periods of equal duration: loading at a constant rate, and retention at the reached level of load. During the periods of loading, the pressure increased by 2 MPa on average and the average rate of the deformation during these periods was 3×10^{-5} 1/s. Unlike in the experiments with small specimen, the block was deformed under the steady stress conditions at the retention stages.

Four through holes 13 mm in diameter were drilled in the central part of the block, along the line oriented at an angle of 30° relative to the vertical axis. These holes served as the concentrators of stresses, providing the area of the internal fracturing developing into the shear macrofracture. The pressure that triggered the failure of the block was 20.4 MPa. However, beginning from as low as 12 MPa, the total deformation increased even under a constant strain, which is indicative of the transition to the nonlinear dependence between the stress and the deformation; the accumulation of the residual strains; and the approaching to the mechanical instability.

Based on the previous analysis of data (local tensometry, location of strong acoustic signals, variations in the

velocities and amplitudes of elastic waves in ultrasonic sounding, electrometry, visual observation of the block through the window in the press chamber), it was inferred that the fracturing in the central part of the block began already after the 8th loading series, under a pressure of approximately 16 MPa, when the shear-type macrofractures that connected the holes–concentrators began to develop [Sobolev et al., 1996].

The final stage of the experiment (18–20 MPa) was accompanied by the formation of numerous fractures near the edges, at the corners, and at the side faces of the block. Taking this consideration, we confined ourselves to the analysis of the acoustic activity within the loading range to 16 MPa, when the failure was to a lesser extent accompanied by local and marginal effects and the flushing.

The acoustic emission signals were measured by two independent multi-channel data acquisition systems. In total, 20 400 acoustic signals were detected. The relatively small amount of detected events is explained by the high threshold of the signal discrimination, due to the acoustic and electric noises.

The acoustic activity decreased during the first four series and then increased up to the end of the experiment (Fig. 11a), which is typical, as was mentioned, in the experiments with uniaxial loading without uniform compression.

Figure 11b presents the normalized curves of the acoustic activity observed under different acting stresses. It is seen that with increasing pressure the peak activity shifts toward the end of the load period and even advances into the interval of the constant load.

The composite plots of the delay of the maximum acoustic activity based on the observation data obtained by both systems are shown in Fig. 11c. This figure displays also the number of acoustic events observed under different acting stresses. It follows from the figure that the dependences of these parameters are similar to their counterparts in the previous experiments with small specimen (Figs. 3, 6). Thus, the revealed regularities persist and even the scale of the experiment (the size of the specimen) changes more than by an order of magnitude.

THE MAIN RESULTS OF LABORATORY MODELING

The performed experiments showed that the stepped initiation may induce the transient processes qualitatively similar to natural events, such as seismic swarms and aftershocks. Smooth steps (in our experiments those with rates of the strain increasing up to 10^{-6}–10^{-5} 1/s) induce the swarm-like acoustic activity. Sharp steps (in our experiments those with rates of the strain increasing at least at 10^{-3} 1/s) result in the seismicity pattern similar to aftershocks. The character and the parameters of the acoustic activity, which reflect the intensity of fracturing, change regularly with the enhancement of the acting stresses and, correspondingly, with the approach of the state of the specimen to the critical one.

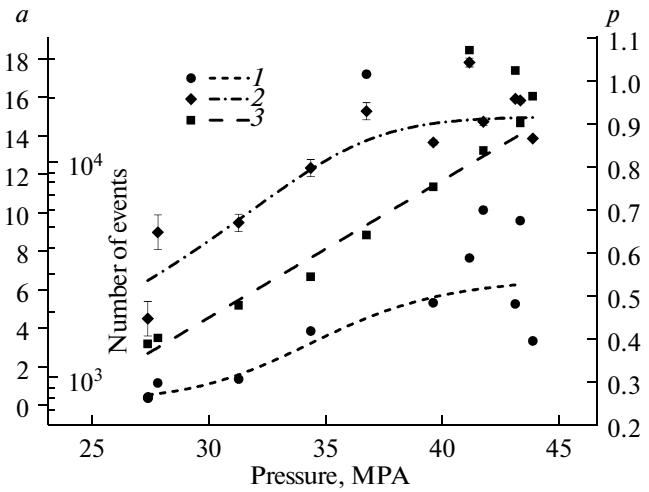

Fig. 10. Parameters of the acoustic regime under different acting differential stresses (experiment A42). Parameters of the generalized Omori's law $\dot{n} = \frac{\dot{n}_0}{(t+a)^p}$: a (*1*) and p (*2*); number of events in each series (*3*), the straight line corresponds to the exponential approximation.

In case of the swarm-like activity, the beginning of relaxation (the beginning of the decay in the activity) occurs later, the higher the acting stresses are. Here under relatively low stresses, the acoustic activity begins to decay already at the stage of growth of the initiating step.[2] This indicates that the initiated activity reflects some self-driving (self-exciting) process, whose parameters are determined by the acting stresses, and the step only triggers this process.

The number of the initiated acoustic events (or the average acoustic activity) exponentially depends on the acting stresses, which is consistent with the kinetic concept of failure (an alternative power-law dependence of the activity on stresses does not agree with the empirical data, which is caused probably by the stepped loading scenario).

Temporal variations in the slope of the frequency-magnitude curves b (at least at the final stages of the experiments, when the acting stresses exceed 60% of the failure threshold) reflect the stages of the growth (excitation) and decay (relaxation) in the acoustic activity: at the growth stage, b decreases, and at the decay stage, it increases. Such variations are qualitatively similar to the changes in the slope of the frequency-magnitude curves at the "excitation" (earthquake preparation) and relaxation (aftershocks) stages of the seismic activity.

In case of aftershock activity, the parameters of the modified Omori's law change with the increase of acting

[2] The experiments on the stepped load of pyrophyllite, greisens, and hard coal samples [Kol'tsov et al., 1984] yielded results, which should be interpreted in terms of the present studies as an increase in the delay of the maximum acoustic activity with increasing acting stresses.

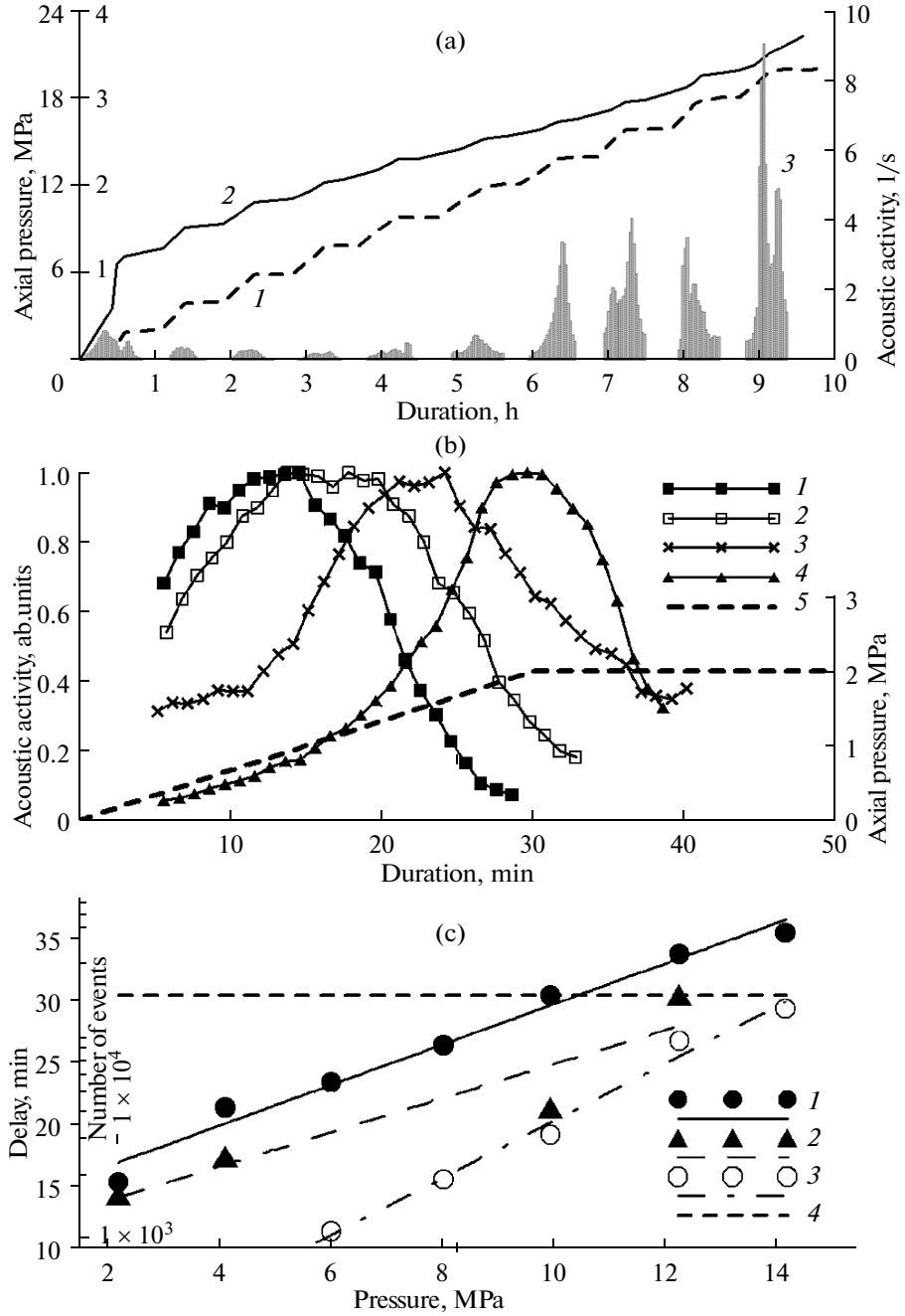

Fig. 11. Experiment LL1 (large limestone specimen): (a) loading history: (*1*) axial stress, (*2*) axial deformation, (*3*) acoustic activity; (b) normalized curves of acoustic activity under different acting stresses: (*1*) 2 MPa, (*2*) 4 MPa, (*3*) 10 MPa, (*4*) 12 MPa, (5) initiating step of the load; (c) parameters of acoustic activity under different acting stresses: (*1, 2*) delay in the maximum activity relative to the commencement of excitation, according to data from two registering systems, (*3*) the number of events in series (the straight line corresponds to the exponential approximation), (*4*) the duration of the period growth of the initiating step.

stresses. The delay of the beginning of the typical power-law decay in the activity increases with an increasing load (similar to the increase of the time interval before the beginning of the decay in the swarm-like activity).

In both cases of the swarm-like and aftershock activity, the slope of the frequency-magnitude curves average over the series increases with the increase in the acting stresses and the development of the specimen failure.

NATURAL EXPERIMENT

Description of the experiment. In this work, we used the data of the natural experiment conducted in Soultz-sous-Forêts in 1993. The experiment consisted of injecting water into the borehole 3-km deep, which induced the local seismicity registered by a special network of stations. The detailed description of the experiment and

measured data are presented in [Cornet et al., 1997; Evans et al., 2005a; 2005b; Evans 2005; Gerard et al., 2006].

The experiment was conducted in the geothermal area composed of dry hot rocks (HDR). Such areas are of commercial interest in view of obtaining geothermal energy by pumping water through deep high-temperature layers. The natural permeability of the rocks is insufficient for reaching a commercial output; therefore, it is used to resort to artificial stimulation when large volumes of fluid are pumped into rocks at high-injection rates. The purpose of this procedure is to increase the pore pressure and to stimulate the failure and dilatancy of natural fractures with the formation of a network of permeable ruptures.

Soultz-sous-Forêts is a test site for the study of hot dry rocks (the European Union's HDT test site). It is located close to the central part of the Upper Rheine Graben, 50 km from Strasbourg. The foundation, divided into blocks, is composed of Hercynian granitoids and rests at a depth of 1400 m, being overlain by the Permian and Hercynian sediments.

In 1992, the previously drilled 2-km-deep Borehole GPK1 was penetrated to a depth of 3600 m. The closely spaced (approximately 800 m away) Borehole EPS1 2227-m deep yielded detailed information on the mode of the strain-stress state and natural fracturing of the massif.

The direction of the axis of maximal jacking strains estimated directly in the borehole by the method of the thermal initiation of failure is 170°NE ± 15°. This value substantially differs from the NW–SE orientation of the axis of the regional stress field, derived from the data about the focal mechanisms of regional earthquakes. The analysis of focal mechanisms of induced seismicity (caused by water injection) implies the presence of both strike-slip and normal slip movements. From this one can infer that the vertical and horizontal compressions are of similar intensity. There are also estimates of the vertical variations in the absolute stresses acting near the borehole.

The casing shoe of Borehole GPK1 is located at a depth of 2850 m; and the remaining 750 m of this well are an open hole 6.25 feet (15.88 mm) in diameter. The borehole penetrates the granite crystalline basement at a depth of approximately 1400 m. The temperature at the bottomhole is 160°C. Detailed logging measurements in the borehole by different methods (ultrasonic, electric, and others), which yielded explicit information on the strain dynamics and fracturing of the walls of the borehole, were carried out prior, during, and after water injection. Preliminary hydraulic testing under low water pressures revealed that the rock permeability is small everywhere near the borehole except for the zone of fracturing, which crosses the hole at a depth of 3490 m. During the experiment discussed here, the well was filled with sand within the depth interval of 3400–3600 m, in order to exclude the intense water discharge through the weakened fractured zone.

Water injection was executed in several stages: in August, September, and October, 1993. At the first stage, the volume of injected water was small, and this stage represents no value for this work. Hydraulic rupturing occurred at the last stage (October, 1993); this stage is also omitted from consideration. The largest volume of water (25000 m^3) was injected into the hole at the second stage (September, 1993). Water was injected stepwise during 17 days, with the fixed injection rate ranging from 0.15 to 36 l/s. Daily well log measurements of the water pumping rate and its temperatures were carried out . Figure 12 presents the plots of water injection and the excess pressure in the hole over the surrounding rock pressure (differential pressure). According to [Evans et al., 2005a; 2005b], the latter exhibits no substantial vertical variations within the open part of the well. The rock pressure at a depth of 2805 m was 28.4 MPa.

Microseismic events during the experiment of 1993 were registered by three four-component accelerometers installed within three abandoned oil wells and by the hydrophone deployed in Borehole EPS1. The aperture of the network was 2 km (the observation wells are located at distances of 0.5 to 1.54 km from Borehole GPK1). The frequency band of the equipment is from 10 to 2500 Hz, and the sampling frequency is 5 kHz. The initial errors of the location of the hypocenter are 20 m in the vertical and 50 m in the horizontal directions. For increasing the resolution, special algorithms were applied. The algorithms are based on the complex of data for groups of events with similar wave characteristics (multiplets). This allowed the location error to be reduced by an order of magnitude. There are intervals of data loss due to the damage of the magnetic tape at the injection "steps," corresponding to pumping water at 12 and 24 l/s.

The seismic catalogue contains information about the time, the coordinates, and the moment magnitudes of microearthquakes. In addition, estimates of the relaxed stresses and the focal size (radius) for all these events derived from the spectral analysis of the waveforms are also available.

In the work [Evans et al., 2005a], the authors report on the general characteristics of seismicity and the structure of the fracturing caused by water injection. The main results of their studies are given below.

(1) A cloud of microearthquakes 0.5 km wide, 1.2 km long, and 1.5 km thick is oriented at 225° NW. One of the most significant structures of the cloud extends downward by 350 m from the water injection point. This structure appeared at the initial stage of injection and likely reflects the main channel of the water drainage from the injection area. This structure is formed by near-vertical strike-slip fractures oriented in the NNW–SSE direction and forming a fault zone 10–20 m wide. This structure probably existed at that place even before the experiment, and its permeability increased due to water injection.

(2) Regular logging measurements during the experiment revealed six zones of enhanced permeability, located at different depths in the open part of the hole.

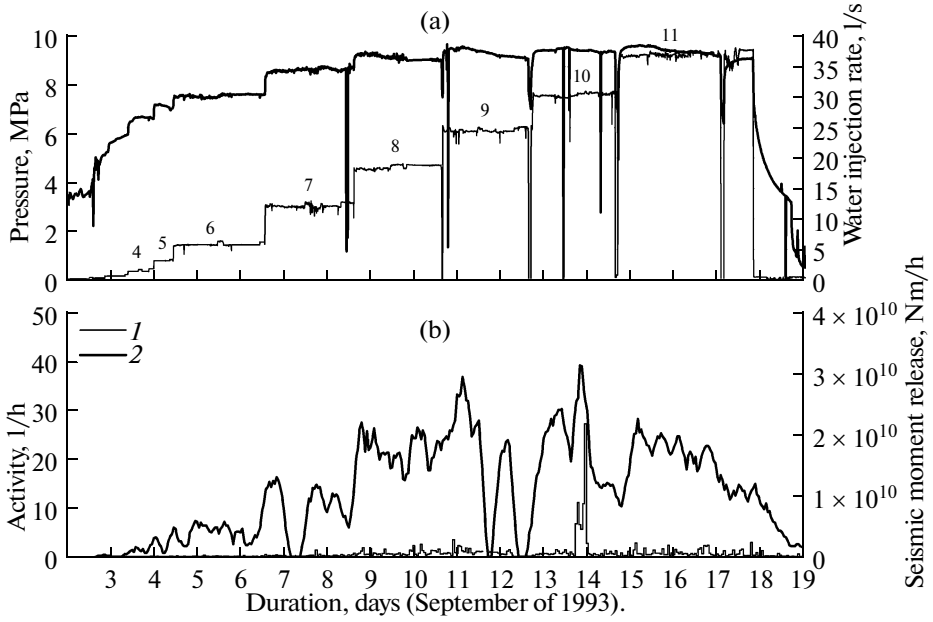

Fig. 12. History of water injection in the natural experiment: (a) water injection rate (*1*) and pressure excess in the hole over the formation pressure (differential pressure) (*2*). Numbers of series used in this work are indicated near the curve of the water injection rate. (b) Parameters of induced seismicity: (*1*) activity (number of seismic events per hour), (*2*) rate of the seismic moment release.

(3) The main structure of the seismicity has a tube-like shape rather than planar. The authors [Evans et al., 2005a] believe that this is explained by the error of location and by the specific method used for its reduction for multiplets. This technique forces the events to migrate toward the "center of masses," which is characterized by the tubular shape.

(4) The analysis of the field of stress indicates that the pore pressure up to a depth of 2900 m (the uppermost part of the open hole) exceeds the minimal horizontal compression beginning from the water injection rate of 18 l/s. For deeper layers, the pore pressure is lower compared to the value of minimal compression. This peculiarity is reflected in the structure of seismicity (and, correspondingly, in the pattern of fracturing). Above 2900 m, the cloud of seismicity extends in the S–N direction, which corresponds to the direction of the axis of stresses; i.e., the structure of the failure is controlled by the jacking stress. Below 2900 m, the seismicity strikes NNS and corresponds to the orientation of the strike-slip fractures that existed prior to the experiment. In this case, the structure of the failure is controlled by the properties of the medium.

(5) The seismicity and, correspondingly, the process of fracturing migrate with time downwards, which cannot be explained by purely hydrostatic factors, since the pore pressure is lower as compared with the minimal compressing stress. Based on the previous models suggested for the swarms of volcanic earthquakes [Hill, 1977], the authors [Evans et al., 2005a] explain this phenomenon by the dynamics of the seismicity itself: the dilatancy-related opening of the strike-slip ruptures, their influence on the neighboring fractures, and, thus, the formation of the vertical channel. In fact, here, we are dealing with the distribution of a certain wave of relaxation oscillations similar to the "domino effect," self-oscillations in the active media, or the waves of seismicity. It should be noted that such phenomena (the gradual growth of the region of fracturing from the nucleation to the "fault" propagation through the entire specimen) was observed also in the experiments on the rocks' failure without fluid injection (an example of such an experiment is given below).

Summarizing this brief review, let us note the items important for the present work.

Prior to the experiment, the geological medium in the region of the borehole was characterized by a grown system of different-scale defects. Water injection stimulated the development of this system due to the fracturing of its elements. Thus, water injection does not form a new system of fracturing but acts as an external factor, which triggers the evolution of the existing complex system of heterogeneities (defects) in the geological medium.

The dynamics of the failure caused by water pumping cannot be explained simply by the dynamics of the fluid. The dynamics of the seismicity is characterized by the internal kinetics related to the processes of deformation and fracturing of the medium, which are only initiated, and not completely determined by water injection (below, we turn back to the detailed discussion of this important question).

All these features allow the experiment in Soultz-sous-Forêts to be considered, to a certain extent, as a model for the transient mode induced (although not con-

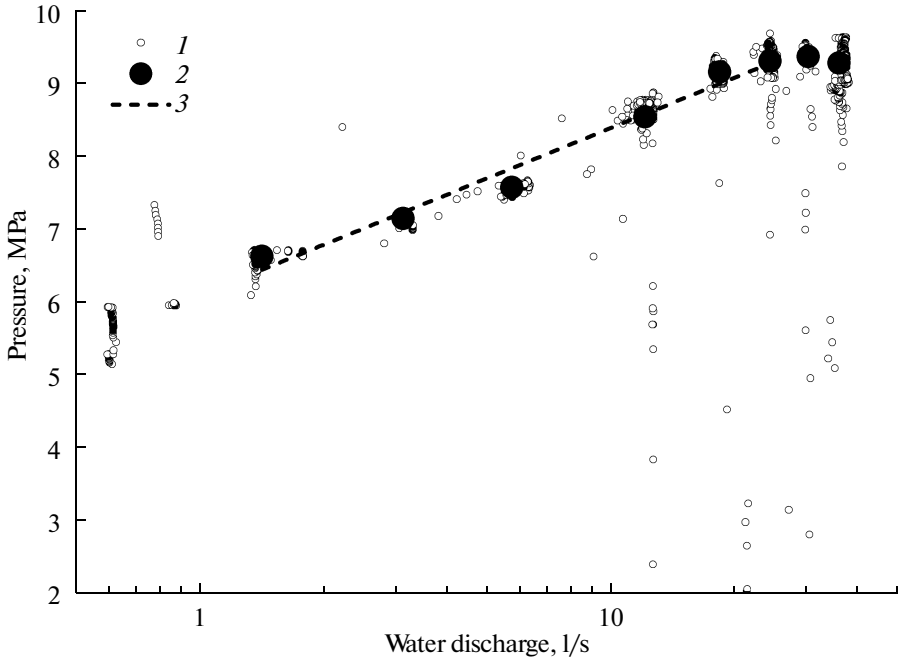

Fig. 13. Water injection rate and pressure: (*1*) initial data, (*2*) average over series, (*3*) approximation $Q \sim e^{\beta P}$.

trolled) by the external impact. In this regard, the results of the natural experiment can be compared with the results of laboratory experiments on the transient modes modeling by excitation of the failure by relatively weak strain impacts. Such a comparison seems to be of critical importance; and it is useful for exploring the possibility for the applicability of the experimental results in studying the regularities and the nature of the process of failure in natural conditions.

Water injection and pressure. Figure 12 illustrates the initial data: the changes in the water injection rate Q, the differential pressure P (excess pressure in the open part of the hole over the surrounding rock pressure), the number of seismic events per hour, and total seismic moment per hour (release velocity of the seismic moment). The seismic catalogue was selected according to magnitudes and its representativeness; the seismic moment (H m) was calculated from the magnitude: $\log M_0 = 1.5M_w + 9.1$.

Let us term the data corresponding to the water injection "steps" as series (by analogy with the laboratory experiments). The series numbers and the water injection rates are indicated in Fig. 12. No seismic events have been observed for the first three series; therefore, they are omitted from further discussion.

Figure 13 presents the scatter plot of the water injection rate and pressure. Beginning from $Q = 18$ l/s (8th series in Fig. 12), the pressure barely increases with the increasing rate of water injection. The authors of the work [Evans et al., 2005a] explain this phenomenon by the increased permeability of the rock due to the development of the failure: it should be noted that according to the estimates in [Evans et al., 2005a], precisely at $Q = 18$ l/s, the pore pressure becomes equal to the minimal compressing stress in the upper part of the open hole segment.

As follows from Fig. 13, at $Q \le 18$ l/s, the dependence of P and Q approaches the linear one in semilogarithmic coordinates. This means that in this interval $Q \sim e^{\beta P}$. If the permeability is assumed to be proportional to the fracturing of the rock material, such an exponential dependence is consistent with the notions of the kinetic concept of failure. Indeed, according to Zhurkov's formula, the probability of failure (the quantity reciprocal to durability) is proportional to $e^{\gamma\sigma}$. Additional stresses σ induced by the water pressure should naturally be considered as being proportional to P: $\sigma = \alpha P$. The fracturing is evidently proportional to the probability of failure; it means that this quantity, as well as the permeability Q will be proportional to $e^{\gamma\alpha P}$, which is illustrated in Fig. 13.

Representativeness of the catalogue. The approach to the assessment of the representative magnitudes is based on the concept of the power-law energy distribution of an earthquake; in this case, the frequency-magnitude relation is linear. If some earthquakes are missed, the points for corresponding classes will lie below the straight line, which determines the known phenomenon of the "bend" of the frequency-magnitude relation in case of small classes. Consequently, the search for the statistically representative class reduces to the solution of the problem of the observed energy distribution of earthquakes, obeying the power-law distribution. In such a statement, the statistical problem was formulated and solved in [Pisarenko; 1989; Sadovskii and Pisarenko, 1991]. Unlike many preceding studies in this field, in his

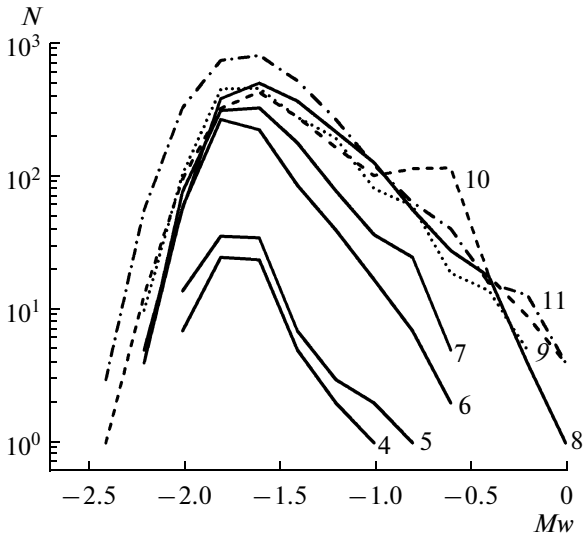

Fig. 14. Frequency-magnitude plots for different series (number of series are indicated near the curves).

work Pisarenko suggested a rigorous statistical solution to the problem, which allows the entire procedure of the analysis to be automatized by specifying only the level of confidence for testing the hypotheses. This technique was implemented in computer programs, and the corresponding mathematical tools make it possible to study the temporal and spatial variations in the representative magnitudes from the catalogues [Smirnov, 1997a; 2004; Smirnov and Gabsatarova, 2003].

The analysis of temporal variations in the representative magnitudes revealed that the threshold for the data selection should be taken as $M = -1.6$. The analysis of the spatial distribution of the representative magnitude shows that this value is representative within the main spot of seismicity.

Figure 14 presents the plots of the frequency-magnitude relation calculated separately for all the series. It is seen that the above estimate of the representative magnitude is valid for all the series. The frequency-magnitude plots are close to linear; only the plot constructed for the 10th series is anomalous, reflecting the anomalous energy release on September 13, which is clearly seen in Fig. 12.

Dynamics of seismic activity. Variations in seismic activity (the number of earthquakes per time unit) are depicted in Fig. 15a. In addition to the expected increase in activity at the transition to higher rates of water injection, the delay of the maximum activity relative to the beginning of water injection into the hole is apparent in the figure. It is also clearly seen that the higher the number of the series, the longer is the delay: the peak activity shift to the right along the time axis.

The duration of the period of increased rate of water injection did not exceed one hour. The delay of the seismic response is substantially longer and, consequently, cannot be explained by this factor. The delay exceeds also the characteristic time of pressure stabilization determined apparently by penetration of the fluid into new regions in rocks (at the transition to higher injection rates). These facts indicate that water movement (diffusion) cannot be considered as a sole mechanism responsible for the delay of the seismic response.

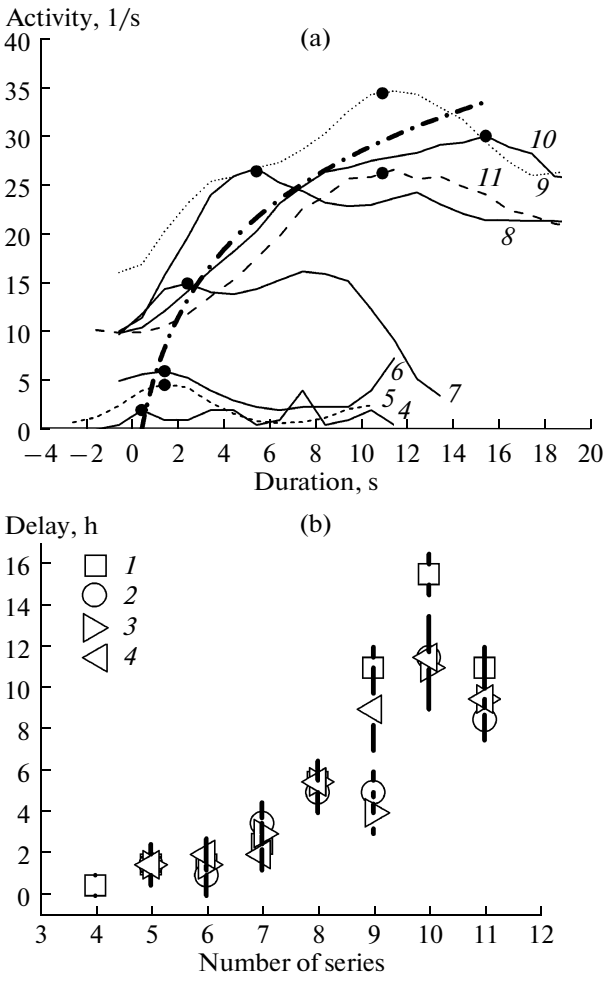

Fig. 15. Seismic activity in the natural experiment: (a) seismic activity for different series based on data from the entire catalogue. Solid dots indicate the maxima in seismic activity for each series; (b) delays in the seismic response for different variants of selection: (*1*) without selection, (*2*) one sphere for all series with the radius of 150 m and the center in the central part of the cloud of seismicity, (*3*) a separate sphere for each series with the radius 150 m and the center in the central part of the cloud of seismicity of the corresponding series, (*4*) a separate sphere for each series with the radius equal to the gyration radius and the center in the central part of the cloud of seismicity of the corresponding series.

The size of the region of induced seismic activity increases from series to series [Evans et al., 2005b; Evans, 2005]. To study the possibility for the influence of the increased seismically active area on the delay of the seismic response, we compared the variations in seismic activity in different samples of the spatial distribution of earthquakes. The idea of this procedure is to compare the delays of seismic responses in areas of fixed and increas-

ing sizes. This allows eliminating the possible artificial dependence of the delay in the response on the size of the area under study. If the delay is caused only by the successive increase in the size of the analyzed area in different series, it should be expected that the delay would remain unchanged in areas with fixed sizes similar for all the series and in areas smaller than the seismogenic region.

As an estimate of the effective radius of the seismically active area the so-called radius of gyration was used. The gyration radius is the root-mean-square of the remoteness of the events, which are the elements of some set (in the considered case, events of a certain series) from the center of the set. The gyration radius can be understood as the estimate of the variance in the approximation of the cloud of events by the Gaussian curve. The following samples of data selection for different series were considered: for all the series, a sphere with a radius of 150 m and the center in the barycenter of the cloud of seismicity (the barycenter is a point, whose coordinates are the average coordinates of the hypocenters of the earthquake); for each series, its own particular sphere with a radius of 150 m and the center in the barycenter of the corresponding series; and for each series, its own particular sphere with the radius equal to the radius of gyration and with the center in the barycenter of the corresponding series. The obtained results are presented in Fig. 15b as the dependences of the delays of peak seismic responses on the series number. The figure displays also the data obtained without spatial selection, which are shown in Fig. 15a. It is seen that regardless of the selection technique, the delay increases with the series number, and the delays corresponding to different selections are close to each other. This allows eliminating the increase in the size of the analyzed area as an artificial factor, responsible for the delay of the seismic response. At the same time, the physical dependence of the delay on the size of the "excited" (seismically active) region of the medium still remains possible.

The analysis of the temporal variations in the gyration radius for each series showed that the extension of the seismically active area begins not immediately upon but 15–20 hours after the jump in the rate of water injection. Within this period the gyration radius remains nearly the same, and the considered peak seismic responses fall (the delays do not exceed 16 hours) precisely in this interval. This confirms the inference about no artificial links between the delay and the increase in the size of the analyzed area.

The following scenario of selection was applied in the eventual calculations: for each series, its own sphere was taken with the center in the central part of the cloud of the series and the radius equal to the radius of gyration. Figure 16 depicts the seismic activity for each series. In Fig. 17, the delay of peak activity is given as a function of the pressure of the injected water. The abscissa axis indicates the values of pressure for the preceding series, i.e., the pressure under which the seismic activity was excited by water injection. The growth of the delay with increasing pressure (i.e., with the enhancement of acting stresses) clearly seen in Fig. 17 is similar to the one observed in the laboratory experiments. It should be noted that when the pressure exceeds the value of the minimal tectonic compression in the upper part of the open borehole segment (let us recall that the pressure reaches this value at the step of the 8th series under $Q =$ 18 l/s, Fig. 12), the delay in the seismic response remains practically the same (last three points in Fig. 17).

To obtain information about the pattern and probable dynamics of the failure process, we have estimated the parameters of the seismic activity for each series. We estimated the slope of the curves of the frequency-magnitude relation, b, the fractal dimensionality of the hypocenters d, and their combination $q = \alpha b - d - \mathrm{d}$, where α is a coefficient relating the energy and the geometrical parameter of the seismic source (its magnitude and size: $M = \alpha \log l + \mathrm{const}$). These statistical values can be used for the estimation of the physical parameters of the rock fracturing based on the seismological data, and, in particular, for estimating the duration of the failure cycle, i.e., the average recurrence period of earthquakes within the region equal to their focal size l [Smirnov, 2003; Smirnov and Ponomarev, 2004]. The parameter q describes the dependence of the duration of the failure cycle τ on l: $\tau = \tau_0(l/l_0)^q$. When $q = 0$, the failure exhibits uniform scale distribution: the probability for the failure of the defect (heterogeneity of rock) does not depend on its size, and the Guttenberg–Richter law is determined only by the distribution of defects in sizes. Such a situation is typical for the background seismicity [Smirnov, 2003]. When $q < 0$, fracturing is more intense at higher scales. Such a situation is typically observed at the initial stage of aftershock sequences; q in the aftershock sequences gradually increases with time, returning eventually to its background value [Smirnov and Ponomarev, 2004]. This implies that the relaxation of the aftershock follows the scenario of the so-called direct cascade of instability, when the intensity of the corresponding process (the failure in our case) is redistributed from higher to lower scales. The inverse cascade is the gradual transition of the failure from lower to higher scales; the reduction of q from positive values to zero corresponds to the inverse cascade. Such a situation was observed during the preparation of some earthquakes [Ponomarev et al., 199]. It corresponds to the scenario of the fractures development due to their interaction and, accordingly, the gradual transition of the failure to higher scales, which is reflected in the concept of the instability of the avalanche crack.

Figure 17 displays the estimates of b, d, and q (in the calculations of the latter parameter it was taken that $\alpha = 2$, according to the type of the magnitude used in the catalogue). The value of b was estimated using the method of maximum likelihood and the d value, using the method of the correlation integral. The decrease in b indicates the enlargement of the seismic events at the transition to the

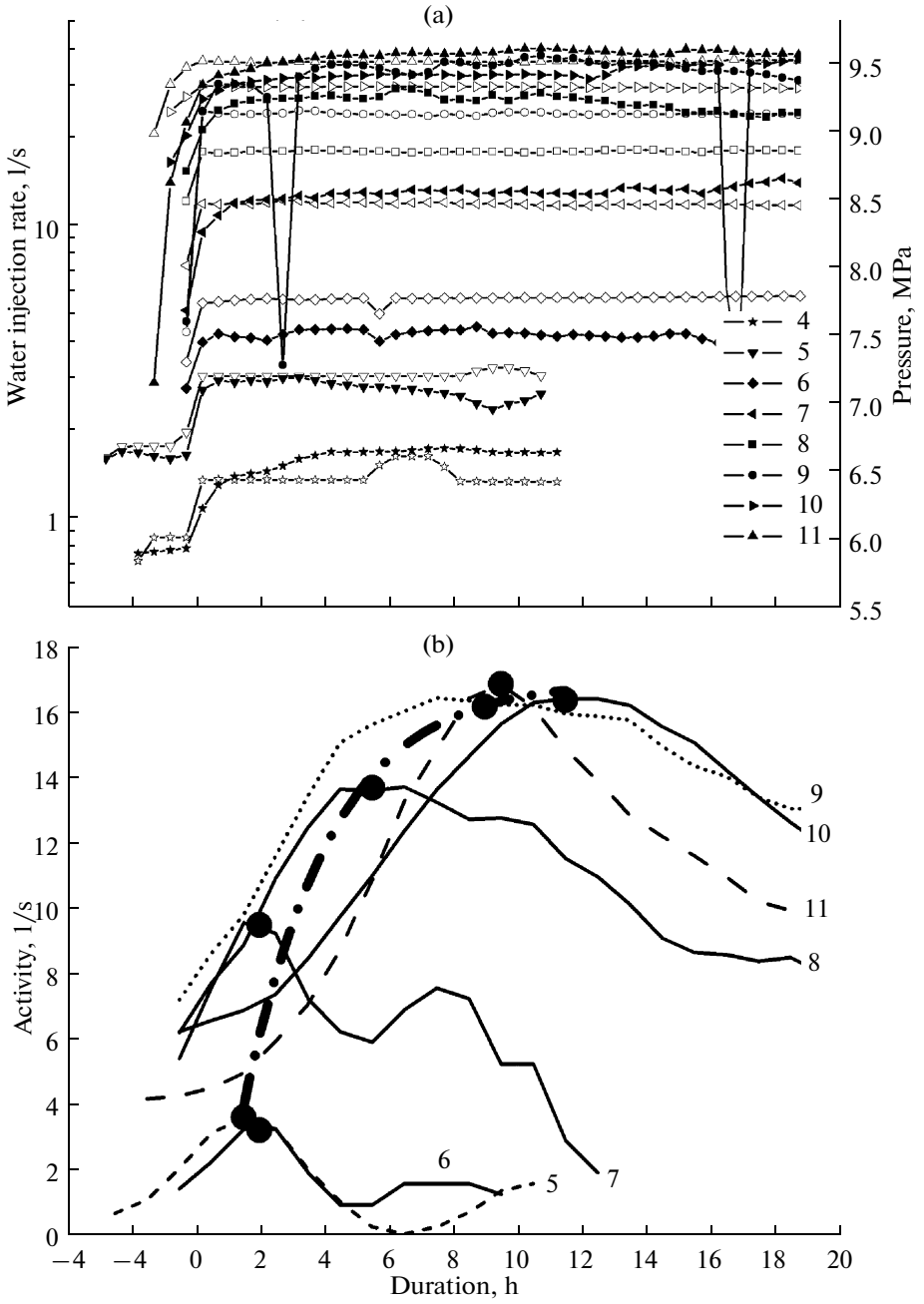

Fig. 16. Water injection and seismic activity in the natural experiment: (a) variations in the water injection rates (open symbols) and differential pressure (solid symbols) for different series. Numbers of curves correspond to the series numbers; (b) variations in the seismic activity for different series based on selected data (series numbers are indicated near the curves). Solid dots indicate the maxima in seismic activity for each series.

higher series. The anomalously high (for the regular background seismicity) value of $b \approx 1.4$, observed in the last series indicates that the process of the formation of the seismogenic structure, typical for the background seismicity of tectonically active regions, has not been completed in the conducted experiment. The faint increase in d from 2.4 to nearly 3 (uniform distribution of the hypocenters in the volume) is probably explained by the presence of a flat weakened zone in the upper part of the open borehole segment at the initial stage of the experiment, and the subsequent expanding of seismicity from this structure into the larger volumes of rocks. Variations in q correspond to the scenario of the transition from lower to higher levels. The plots of the frequency-magnitude relations (Fig. 14) confirm this inference. This figure shows that the lower series are lacking in relatively strong events, which appear gradually in the higher series. Such a situation is observed in the experiment

[Smirnov et al., 1995; Ponomarev et al., 1997; Tomilin, 1997] with the gradual formation of the macroscopic zone of failure and is interpreted in terms of the concept of fracture enlargement resulting from their interaction (crack instability avalanche scenario).

Figure 17 depicts the entire number of earthquakes in each series. Similar to the laboratory experiments, the dependence of the number of events on pressure is well approximated by the exponent.

Figure 18 presents the temporal variations in the slope of the frequency-magnitude plots (*b*) for the last three (9–11) series; for the earlier series, the statistics of events is insufficient for the study of temporal variations in *b*. A similar pattern of variations in *b* is observed, which allows averaging the data over different series, for a higher reliability of the results. It is apparent in the figure that the stages of higher seismic activity correspond to a lower *b*, and lower activity, to a slightly increased *b*. The statistical reliability of the observed changes in *b* is not high; however, the revealed trend implies that excitation is implemented through the transition of fracturing from lower to higher levels (inverse cascade, crack instability avalanche scenario); and relaxation, through the transition of fracturing from higher to lower levels (direct cascade, scenario of aftershocks). Laboratory experiments yielded similar results (Fig. 7).

Multiplets. Bourouis and Bernard [2007] defined and analyzed the groups of earthquakes called multiplets. Each multiplet comprises events with repeated (practically similar in shapes) seismograms (the coefficient of correlation of the seismograms exceeds 0.9). It was mentioned above that the analysis of the seismograms of all events in the multiplet as a whole made it possible to increase significantly the accuracy of their location.

The authors of the cited work interpret each multiplet as the repeated acts of fracturing of the same heterogeneity, or asperity (in the authors' terminology; further, we use the term "heterogeneity"). The presented multiplets contain from two to 75 events. The focal spectra of the events of each multiplet are similar in shape but different in amplitudes; correspondingly, the events of the multiplet have different magnitudes. The temporal distribution of the events within the multiplet obeys Omori's law (at least at the initial stage), which confirms the idea of the implementation of the failure of the "excited" heterogeneity in the multiplet events.

The catalogue of multiplets contains information about 4825 events that form multiplets each consisting of 2 to 75 events (let us designate the number of events constituting the multiplet as its rank) and 4334 singlets (the events that do not enter into any multiplet). The rank distribution (rank 1 corresponds to singlets) of the low-rank multiplets (approximately lower than 15) is governed by the power law. The number of multiplets of ranks higher than 15 is insignificant (one–two) and is rank independent.

If each multiplet is considered as a manifestation of the process of the heterogeneity fracturing, it is possible

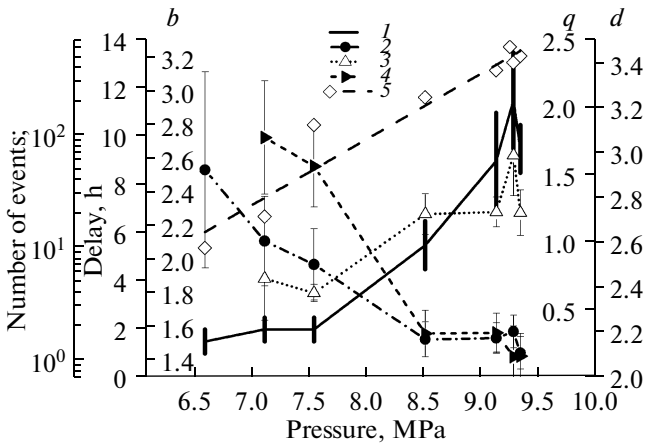

Fig. 17. Parameters of the seismic regime depending on the pressure of injected water: (*1*) delay in the maximum activity, (*2*) the slope of the frequency-magnitude plot, (*b*; *3*) fractal size of the set of hypocenters *d*, (*4*) parameter *q*, (*5*) total number of earthquakes in series; the straight line corresponds to the exponential approximation.

to estimate the size of the heterogeneity and the duration of its "activity" from the multiplets. Let us take the gyration radius of the cloud of events constituting the multiplet as a measure of heterogeneity. The gyration diameter $D_g = 2R_g$ defines the area that includes (in case of the Gaussian distribution) approximately 66% of events, and the doubled giration diameter, 96% of events. Let us take the latter value as an estimate for the size of the heterogeneity: $L_a = 2D_g = 4R_g$.

Figure 19a presents the estimates of L_a calculated for each multiplet and those averaged over the multiplets of the same rank. Also, the values are shown of L_m equal to the doubled distance from the barycenter of the cloud of

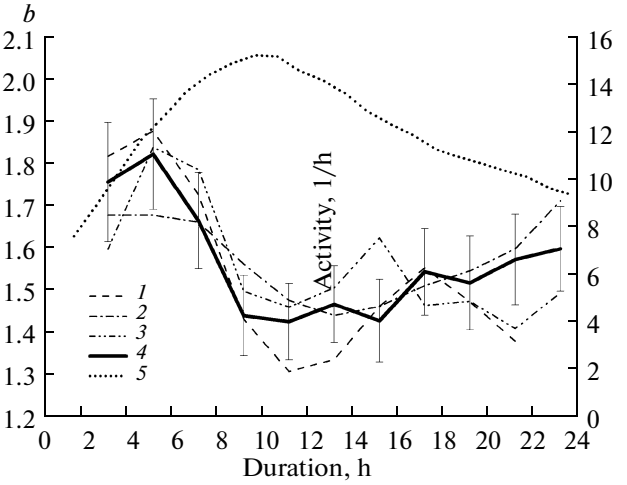

Fig. 18. Temporal variations in the slope of the frequency-magnitude curves *b* within series: (*1*) 9th series, (*2*) 10th series, (*3*) 11th series, (*4*) average for three series, (*5*) average activity for three series.

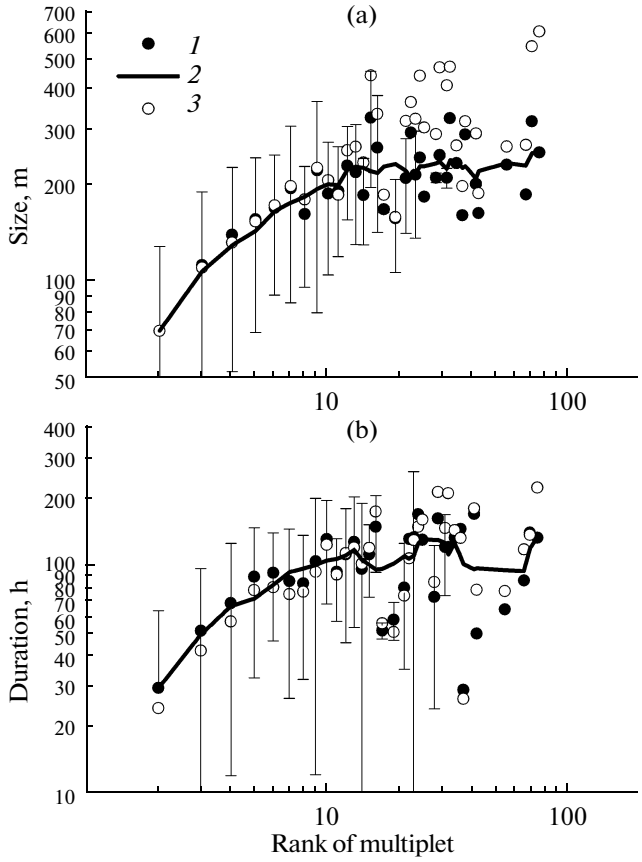

Fig. 19. Dependence of the size of heterogeneity (a) and the duration of its activity (b) on the rank of multiplet: (*1*) L_a and T_a estimates, vertical lines indicate the scatter of estimates in the group of similar-rank multiplets, (*2*) smoothing of L_a and T_a estimates, (*3*) L_m and T_m estimates.

multiplet events to the remotest event of this multiplet. It is seen that the estimates of L_a are close to the "maximal diameter" of the cloud L_m. However, we consider the L_a estimates as being preferable because they are statistically more stable compared to the estimates of the "maximal diameter": the latter are based in fact on a single point determinations (the event located at the maximal distance from the barycenter), while L_a is estimated from the entire set of data.

By analogy with the size of heterogeneity, let us estimate the duration of its "activity" using the standard deviation (square root of the variance) of times T_g of the events from the given multiplet. The duration of the interval T_a, corresponding to the duration of the activity of the given heterogeneity can be expressed in terms of T_g. In case of the Poisson process, the times of the events are uniformly distributed within the interval T; the variance of this distribution is $T^2/12$, and the standard deviation, correspondingly, $T/2\sqrt{3}$. Thus, the duration T_a is estimated as $2\ T_a = 2\sqrt{3}\,T_g$. Figure 19b presents the estimates of T_a calculated for each multiplet, and the values averaged over the multiplets of the same rank. The figure shows also the durations of the multiplets estimated as the difference between the times of the first and the last events of the multiplet (which are in turn also averaged over the multiplets of the same rank). It is seen that the values of T_m and T_a agree with each other, although the T_m estimates seem to be preferable as being statistically more stable.

Figure 19 shows that in that area of the multiplet ranks, where their distribution obeyed the power-law (below the 15th rank), the average size L_a and the average duration T_a of the multiplet increase with its rank, while these parameters of the higher rank multiplets remain approximately the same. It is difficult to say whether this regularity has a physical sense, or results from the procedure of determination of the multiplet and grouping of the data, that is, artificial dividing of the heterogeneities into classes based on the amount of the events related to the given multiplet (i.e., grouping according to the rank of the multiplet).

It follows from Fig. 19 that the scatter in the estimates of L_a and T_a within the group of multiplets of the same rank is noticeably larger compared to the difference of the average values for the ranks. Hence, it seems reasonable to consider the general statistics of the heterogeneities without their subdivision in the ranks of multiplets.

Figure 20 illustrates the distribution of heterogeneities in sizes regardless of the ranks of their multiplets. For comparison, also the magnitude distribution of all the registered microearthquakes (singlets included) is presented. In the abscissa axis, the scale of magnitudes is combined with the scale of the heterogeneity sizes according to the relation $M_w = 2\log L_a - 1.92$ [Smirnov, 2003]. This relation agrees well with both the magnitude and energy estimates of the focal sizes of earthquake [*Earthquakes* ..., 2006; *NMSOP* ..., 2002].

The size distribution of the heterogeneities is similar, with the typical distributions of lithospheric heterogeneities of different scales: faults, crustal blocks, lithospheric plates, and others [Sadovskii et al., 1987; Cladouhos and Marrett, 1996; Nicol et al., 1996; Watterson et al., 1996; Yielding et al., 1996; Smirnov and Feofilaktov, 2000a; 2000b; Bird, 2003; Sornette and Pisarenko, 2003; Goto and Otsuki, 2004; Golitsyn, 2008]. The power-law approximation of the descending branch of the distribution $\log N = -d\log L_a + \text{const}$, based on the concept of structural self-similarity of the lithospheric heterogeneity, yields the estimation of the self-similarity index as $d_a = 1.6$. This value, rendered into the seismological "units" via a formal transition from L_a to M_w, provides the slope of the "frequency-magnitude" plot with respect to asperity $b_a = 0.8$. This value is close to the typical "global average" (0.9) of the Guttenberg–Richter parameter, although substantially lower than the slope of the frequency-magnitude curve for the seismicity induced by water injection that changes from 2.5 at the beginning to 1.4 at the end of the experiment.

The interrelation between the indices of energy self-similarity of the seismicity and geometric self-similarity of lithospheric heterogeneities is the subject of long discussion [Aki, 1981; King, 1983; Grigoryan, 1988; Turkott, 1992; Smirnov, 1997b; Bak et al., 2002; Coral, 2005]. The known relation $b = d/\alpha$ may be considered as the result of a certain consistency between the structure of the failure and the structure of the heterogeneities in the medium, when the energy distribution of earthquakes is entirely determined by the size distribution of the heterogeneities and by the correlation between the energy of the earthquake with the size of the fracturing heterogeneity. In this case, the probability of the failure of different-size heterogeneities proves to be constant. Such a situation is typical for the background seismic activity, but is sharply violated in transient modes [Smirnov, 2003; Smirnov and Ponomarev, 2004]. If we take the above derived estimate d_a as the estimate of the index of self-similarity for the structure of heterogeneities in the region of the experiment, the relation $b = d/\alpha$, in our case, also becomes disturbed: even the minimal value $b = 1.4$ reached at the end of the experiment is too high as compared with $d/\alpha = 0.8$ (α in our case is 2). This suggests a "deficiency" of strong seismic events.

The laboratory studies show that the increased values of b and, correspondingly, the "deficiency" of strong events are typical of the initial stage of the formation of the failure zone [Zhurkov et al., 1977; Kuksenko, 1986; Main et al.,1989; Smirnov et al., 1995; Ponomarev et al., 1997; Tomiilin, 1997; Scholz, 2002]. The subsequent gradual enlargement of the fractures due to their interaction (when the stress fields overlap near the tips of the fractures) and their fusion is accompanied by the transition of failure from lower to higher scales, the appearance of successively stronger events, and the decrease in the slopes of the frequency-magnitude curves. In the considered natural experiment we observed the same situation: the slope of the frequency-magnitude plot decreases with the development of failure initiated by water injection, although it remains below the level corresponding to the structure of the heterogeneity of the medium heterogeneity (in our case, $d_a/2$). This can be interpreted as an indication of the fact that the structure of fracturing had not matured completely during the experiment: the water pressure and, probably, the duration of its impact are likely insufficient for the transformation of the region of the experiment into the state characteristic of tectonic regions with well-developed background seismicity.

For defining the dynamics of the clustered induced seismicity, the catalogue of multiplets was subjected to the same analysis as the initial (complete) catalogue. As in the case of complete catalogue, the earthquakes were selected within the spheres with the centers in the barycenter of the cloud of the series and the radius equal to the gyration radius. The variations in the activity of clustered events are similar to the variations in seismic activity as a whole: the delay of the maximum activity relative to the beginning of water injection into the borehole increases with the increase in a series number. In Fig. 21,

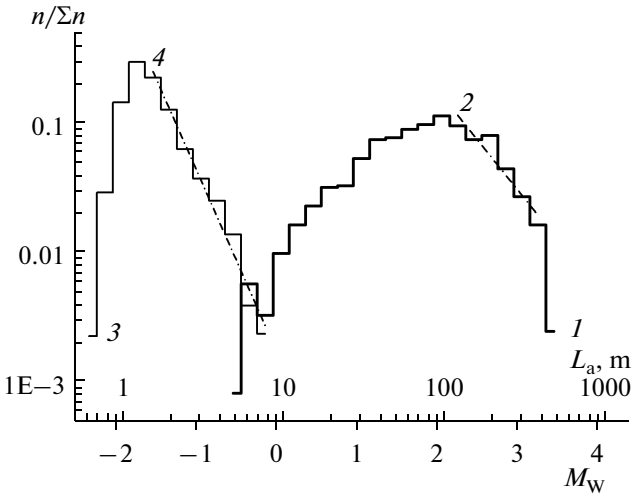

Fig. 20. The size distribution of heterogeneities (1) and the magnitude distribution of earthquakes (3), (*2*) power-law approximation of the descending branch of the size distribution of heterogeneities, (*4*) the Gutenberg–Richter law approximation of the earthquakes distribution .

the delays and the slopes in the plots of the frequency-magnitude relations obtained from the multiplets are combined with the results derived from the entire catalogue (Fig. 17). It is seen that the difference is insignificant and not essential: the main patterns in the dependence of the delay and b on the injected water pressure (and, correspondingly, local stresses) are observed also in the clustered induced seismicity.

Diffusion. The nature and the mechanisms responsible for the increase in the size of the region of induced seismicity are of significant importance for the problem in question. Does failure precede the penetration of water that fills the fractured areas of the medium; or, on the contrary, the failure follows the front of water diffusion? In fact, this is the question concerning the nature of the kinetics of the extension of the region involved in the developing fracturing: is this enlargement determined by the kinetics of the failure itself, or does it simply reflects the kinetics of water motion? And if both mechanisms work, how can the contribution of each of these mechanisms be estimated?

In the work [Shapiro et al., 1999], the increase in the size of the region of induced seismicity R with time t in the experiment under consideration is approximated by the following "diffusion" dependence

$$R = \sqrt{4\pi Dt} \qquad (2)$$

and is explained by water invasion. Similar conclusions are also drawn for other experiments on water injection into boreholes [Shapiro et al., 1997; Audigan et al., 2002]. Formula (2) corresponds to the equation of the so-called second type Biot wave for excitation of the pore pressure of liquid in the low-frequency approximation:

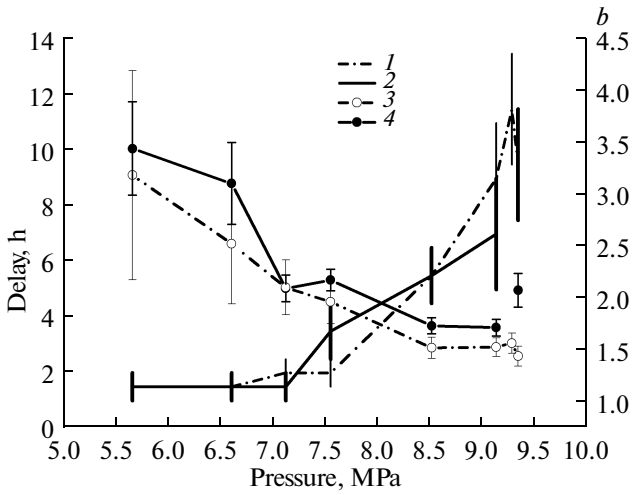

Fig. 21. Delay in the response and the slope of the frequency-magnitude curve b depending on water pressure based on the data from the entire catalogue and multiplets. Delay: (*1*) inferred from the entire catalogue, (*2*) inferred from the catalogue of multiplets; the slope of the frequency-magnitude curve: (*3*) inferred from the entire catalogue, (*4*) inferred from the catalogue of multiplets.

$$\frac{\partial p}{\partial t} = D\nabla^2 p. \qquad (3)$$

In [Shapiro et al., 1999], the approximation (2) is derived from the dependence of the maximal distance between the water injection point (the lower, open part of the borehole) and the hypocenters of induced microearthquakes on the time lapse after the commencement of the experiment. Then, the authors generalize equation (3) to the case of a medium with anisotropic permeability, and obtain the estimates for the corresponding tensor of diffusion.

The purpose of the work [Shapiro et al., 1999] was to assess the effective permeability of the fractured area; and the authors simplified the task in accordance with their aims. The following issues emphasized in [Shapiro et al., 1999] are of principal significance for us. The stresses caused by both the water injection and aseismic displacements propagate faster than the front of the diffusion of the fluid moves (the front of pressure relaxation in (3)). These stresses cause earthquakes (we mean the triggering mechanism) in a as yet unfractured area, thus forming the wave of failure, which runs ahead of the wave of the pore pressure relaxation. The wave of failure changes the permeability of the medium, the D value becomes no longer constant, and equation (3) becomes nonlinear. The authors [Shapiro et al., 1999] ignored these effects and thus reduced the failure to a "passive" process, which reflects simply water movement. Cornet [2000] subjected this simplification to criticism believing that the latter changes principally the essence of the problem.

In order to form our own view concerning the pattern and the nature of the expansion of the zone of fracturing and its consistency with the diffusion model, we analyzed the growth of the seismogenic area with time. We used the catalogue containing only the representative earthquakes (in [Shapiro et al., 1999], the question of representativeness remained beyond discussion: probably, no selection was performed). To characterize the size of the seismogenic area, we used the radius of gyration with respect to the barycenter of the cloud of microearthquakes within each period of time (instead of the maximum distance of microearthquakes from the water injection point used in [Shapiro et al., 1999]). As mentioned above, the radius of the gyration is a statistically more stable estimate, while the fixation of the "center of diffusion" in the point of the hole seems disputable since in the course of the development of fracturing the liquid may be injected from other points through the formed channels of enhanced permeability (the "center of diffusion" may migrate within the fractured area).

For the convenience of comparison, let us assume that the radius of the cloud relative to its barycenter is $R = 2R_g$. The time dependence of R is shown in Fig. 22a. This figure presents also the distances between the holes and the hypocenters of microearthquakes (by analogy with the work [Shapiro et al., 1999]) and the distances between the borehole and the barycenters of the clouds of earthquakes. The figure reproduces also the curve (*3*) with $D = 0.05$ m^2/s from [Shapiro et al., 1999]. Figure 22a is similar to Fig. 1 from the latter work, and the diffusion approximation of the maximum distances between the holes and the hypocenters of the microearthquakes (*3*) seems at first sight acceptable.

A more detailed notion about the correlation between the size of the seismogenic zone and time can be obtained from Figure 22b, where the same data as in Fig. 22a are presented on a logarithmical scale. It is seen here that at the beginning of the experiment, within approximately the first 100 hours, the displacement of the barycenter of the cloud of seismicity is comparable with its size. This means that the model with a single point center of diffusion used in [Shapiro et al., 1999] is inapplicable within the period of the first 100 h (which is emphasized in [Cornet, 2000]). During the period from 100 to 360 h, the diffusion approximation (2) is not quite consistent with the observed data: the slope of the straight line (*3*) is underestimated. Thus, the simple "diffusion" explanation to the enlargement of the seismogenic area proposed in [Shapiro et al., 1999] can be considered as valid only as a rough approximation.

Figure 22 presents the power-law approximation for the time dependence of the size of the earthquake cloud yielded by the formal regression $\log R$ in $\log t$ within the period from 100 to 360 h. The exponent c in $R = At^c$ proved equal to $c = 0.88 \pm 0.03$, which significantly exceeds the value 0.5 corresponding to the pure diffusion in case of the hydrodynamic mechanism.

In our opinion, the more rapid growth of the seismogenic area is indicative of the other mechanism of the development of the fractured zone, which acts solely or in addition to the hydrodynamic one. The kinetics of fracturing may be such a mechanism. The specific example is discussed in the works [Evans et al., 2005b; Evans, 2005; Bourouis and Bernard, 2007]. As was mentioned, these works note that the water pressure reaches only the minimum values of compressing tectonic stresses, only in the uppermost part of the open segment of the borehole, and only at the final stage of the experiment, which increases the doubts on the possibility of a purely hydrodynamic explanation of the development of the failure.

The possibility of the gradual diffusion-like enlargement of the zone involved in fracturing with no participation of liquid at all is confirmed in the laboratory experiments. The results obtained in one of such experiments conducted in the Rock Friction Laboratory (USGS) are presented below. The data yielded by a series of experiments, including the one mentioned above, were analyzed many times [Lockner et al, 1991, 1992; Reches et al., 1994; Smirnov et al., 1995; Sobolev and Ponomarev, 1999]; these works provide a detailed description of the instrumentation and methods used in the experiment (in the last two works, the experiment under consideration is designated as AE42).

A dry Westerly granite specimen was subjected to uniaxial loading under uniform compression. A special regime of loading under the acoustic emission rate feedback control made it possible to conduct a detailed study of the nucleation and development of the failure. The parameters of loading were controlled during the experiment. The special system of sensors mounted on the specimen allowed locating the sources of the acoustic events and compiling their catalogue, similar to the catalogue of earthquakes in natural conditions.

Until a certain stage, while the distances between the microfractures substantially exceed their sizes, fracturing is uniformly distributed throughout the specimen. With the increase in the density of microfractures, the distances between them decrease, and the stress fields concentrated at the tips of fractures become overlapping, which leads to the interaction of the fractures. This results in the grading of the failure into the stage of localization: a small area (the "nucleus" of the macroscopic facture) is formed inside the specimen, where the process of fracturing is concentrated; the acoustic activity outside this area sharply decreases. Then, the size of the "nucleus" area gradually increases: as the failure develops, this area grows forming a narrow zone close to the plane of maximum Coulomb stresses. The regime of loading is such that this growth occurs under stresses nearly constant in time. If the loading continues, this narrow zone of failure crosses the entire specimen, thus, forming a macroscopic fault.

Figure 23 illustrates the time dependence of the size of the failure zone. This dependency is derived from the data of the acoustic catalogue (the above-mentioned methods were used). The regression in the form $R = At^c + R_0$ (the summand R_0 is added to allow for the nonzero initial size of the "nucleus" failure area) yields the following relation: $c = 0.6 \pm 0.2$, $R_0 = (23 \pm 7)$ mm. Thus, the dynamics of the area of the failure are close to the diffusion dynamics, although it should be emphasized again that no liquid was used in the experiment. This example indicates that the kinetics of the process of failure may provide the same results as the dynamics (diffusion) of liquid. Therefore, the question concerning the nature and mechanisms, responsible for the enlargement of the seismogenic area of induced seismicity in the Soultz-sous-Forêts experiment, in our opinion, remains unsolved.

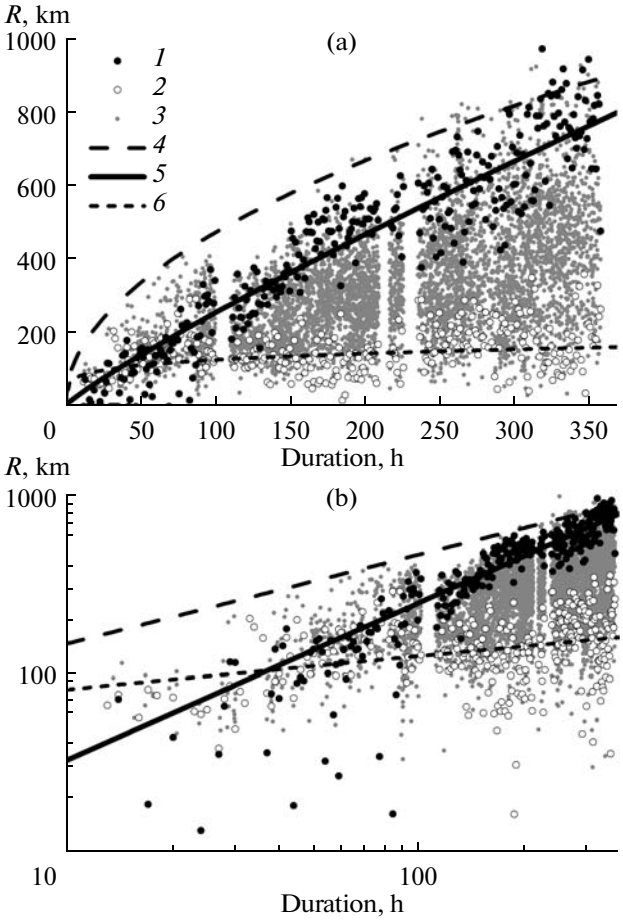

Fig. 22. The size of the cloud of seismicity as a function of time from the beginning of the experiment on the linear (a) and logarithmic (b) scales: (*1*) size of the cloud estimated from the gyration radius, (*2*) distance from the borehole to the center of the cloud, (*3*) distance from the borehole to hypocenters of earthquakes (by analogy with [Shapiro et al., 1999]), (*4*) diffusion approximation $R = \sqrt{4\pi Dt}$ at $D = 0.05$ m^2/s from [Shapiro et al., 1999], (*5*) power-law approximation of the size of the cloud, (*6*) power-law approximation of the distance between the borehole and the barycenter of the cloud.

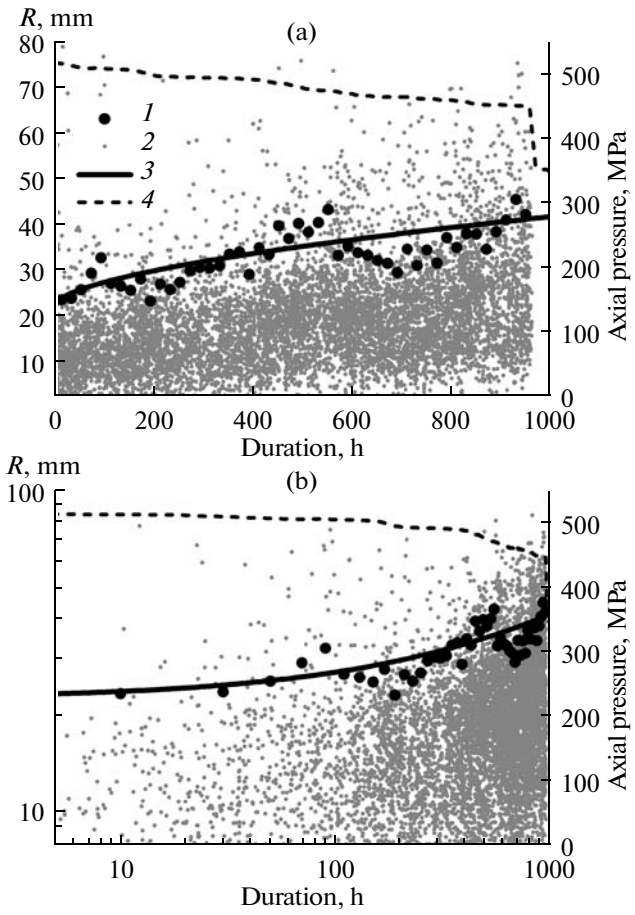

Fig. 23. The size of the cloud of seismicity as a function of time from the commencement of nucleation on the linear (a) and logarithmic (b) scales: (*1*) size of the cloud estimated from the gyration radius, (*2*) distance between the center of nucleation and the hypocenters of the acoustic events, (*3*) power-law approximation of the size of the cloud (the initial size of the nucleation "embryo" taken into account), (*4*) axial stress provided by the press.

MAIN RESULTS OF THE NATURAL EXPERIMENT

Let us note the results, which are of interest for this work: water injection induces swarm seismicity; the stronger the local stresses, the later the relaxation (the decay of the activity) starts; the time changes in the slope of the frequency-magnitude curve for induced swarms of microearthquakes imply that excitation is implemented through the transition of the failure from the lower to the higher levels (inverse cascade, the crack instability avalanche scenario), and the relaxation, through the transition of the failure from the higher to the lower levels (direct cascade, scenario of aftershocks). These data obtained in natural conditions are similar to the results of laboratory experiments, which support their use for studying the regularities and the nature of the transient modes of seismicity.

INTERPRETATION AND MATHEMATICAL ILLUSTRATION

General (physical) reasoning. The obvious idea to explain the regularities revealed in the experiments is the following: the dynamics of the failure induced by the external impact (i.e., the nature of the transient mode) is determined through the competition of two processes: excitation and relaxation.

Excitation (development of the failure) is controlled by the stability and interaction of fractures, which is determined primarily by the level of acting stresses, the structural peculiarities of the medium (concentration of defects, their geometry) and physicochemical factors (the amount and properties of the fluid, temperature, electromagnetic fields, and others). The results yielded by the experiments indicate that excitation develops in accordance with the scenario of the inverse cascade: the failure is transferred from smaller to larger scales, which is typical of the "ordinary" (without the external impact) development of seismicity, including the processes of earthquake preparation. In the last case, the avalanche development of the failure occurs. It is possible that the same physics of excitation may result in both avalanche and nonavalanche development (similar to the explosive and controlled chain reaction). To date, the factors determining the degree of avalanche excitation remain unclear. We may only suggest that they are connected with both the conditions controlling the internal development of the avalanche and the intensity and characteristic time (rate) of the exciting impact.

The nature of relaxation is less clear. This may be both the "passive" relaxation of stresses via various dissipative mechanisms (viscosity, plasticity, friction, and other creep phenomena) and "active" relaxation via subsequent events (energy dissipation during the failure of the material). Both these mechanisms may act simultaneously.

The intensity of excitation nonlinearly depends on stresses (or other governing parameters); both exponential and power-law dependences are known. Under relatively low stresses, the excitation is weak; therefore, the relaxation begins earlier. Under significant stresses the excitation is substantially more intense; it noticeably exceeds the relaxation, and the regime of relaxation forms later, sometimes after the cessation of the increase of loading. This may explain the dependence of the commencement of relaxation on the load, which was established in the experiments.

Mathematical illustration. To illustrate the above mentioned general notions, let us consider the simplest mathematical model. Assume that at each level of stress the medium contains overstressed regions favorable for the development of failure: some portions of the medium reside at the metastable state, and their constituting defects are ready for failure. We will call the set of such overstressed areas as a reservoir of failure (in the sense that the events of failure, or acts, originate from this reservoir). Let the size (capacity) of the reservoir be A. This

value increases, the higher the level of acting stresses.[3] Application of small additional stresses (steps in the described experiments) triggers the avalanche failure. When all the metastable defects fail in all the overstressed areas, the failure process terminates.

The notion of the presence of the reservoir of failure defined by the level of applied stresses is close to the idea explaining the Kaiser's effect (for the review on the problem, see [Lavrov et al., 2004]). In our work, we, however, left aside Kaiser's effect and focused at the commencement of relaxation rather than at the excitation of failure. The question concerning the possible role of memory effects in the dynamics of the transient mode seismicity requires special studies, including special experiments. This issue is a particular case of the more general principal problem of the description of the time factor during the failure in the geological medium.

The capacity of the reservoir decreases as the failure develops. we assume that this decrease is proportional to the number of failure acts n. In this situation, the current size of the reservoir is $(A - kn)$.

Under avalanche failure, the intensity of fracturing (the number of events within the given period) is proportional to the number n of events that had already occurred (probably, in some power of β). The intensity is also proportional to the capacity of the reservoir $(A - kn)$: the larger the reservoir, the greater the number of avalanches that may appear. Thus:

$$\frac{dn}{dt} = R(A - kn)n^{\beta}. \quad (4)$$

We write out (4) in another form:

$$\frac{dn}{dt} = r\left(1 - \frac{n}{a}\right)n^{\beta}, \quad (5)$$

where a is the capacity of the reservoir in units of the failure acts. In the scope of the model, a is determined by the acting stresses (the pattern of the dependence at this level of the analysis is insignificant; only the fact that the stronger the strains the higher the a value is of importance.

Equations of type (5) are known in different fields of knowledge [Svirezhev, 1976; Romanovskii, 1984; Malinetskii and Potapov, 2002; Riznichenko, 2003; Samarskii, 2005]. In the population growth theory, equation (5) with $\beta = 1$ is known as Verhulst's equation (or the logistic equation) [Vogels, 1975]. It describes the growth in population with limited resources for the maintenance of reproduction. The parameter a is called the medium capacity or population capacity; it is defined by the available resources. Our idea of the limitation of the failure by the reservoir containing the metastable defects is, in fact, similar to this concept.

[3] The capacity of the reservoir may depend on other factors as well, including stress duration. At present, we do not include these factors in the model because their contribution has not been studied in the performed experiments.

Equation (5) may be presented in a different form:

$$\frac{dn}{dt} = rn^{\beta} - \frac{r}{a}n^{\beta+1}. \quad (6)$$

The first and second summands in (6) describe excitation and relaxation, respectively; the coefficient a is the ratio of excitation and relaxation: the higher a, the more important is the role of excitation. Equation (6) may be generalized as:

$$\frac{dn}{dt} = pn^{\beta} - qn^{\alpha}. \quad (7)$$

In this case, the proportion of excitation and relaxation is determined by the p/q value.

The equations of type $\frac{dn}{dt} = cn^{S}$ are known as equations describing the blow-up processes [Malinetskii and Potapov, 2002]. In the general case, their solutions are characterized by the power-low asymptotics and describe both the modes of excitation (at $c > 0$) and relaxation (at $c < 0$). Some researchers [Malyshev and Tikhonov, 2007] used such equations in describing the dynamics of seismicity. In the latter work, the authors estimate s. In the context of assumptions made in [Malyshev and Tikhonov, 2007], the characteristic value of s proved close to 2. The value $s = 1$ corresponds to exponential growth (relaxation), when the increase (decrease) is defined only by the total number of events (n) at the given instant of time. Such a situation corresponds to independent events. If the occurrence of a single event changes the probability of the following event (i.e., the interaction between the events becomes important), the value of s may differ from unity (such as, for example, in case of autocatalytic chemical reactions). The value s close to 2 indicates the substantial contribution of interactions between earthquakes, which is consistent with the present-day notions of the physics of seismicity.

Application of the additional step of stress $f(t)$ (such a regime was implemented in our experiments) results in the increase of the dn/dt. The exact dependence of the dn/dt on f is not known. Nevertheless, taking into account the smallness of the additional stress compared to the acting stresses, we may assume that dn/dt is proportional to $f(t)$. Hence, the working model takes the following form:

$$\frac{dn}{dt} = r\left(1 - \frac{n}{a}\right)n^{\beta} + f(t). \quad (8)$$

In our experiments, $f(t)$ was represented by a function linearly increasing within the time interval τ. Thus, the final model is:

$$\begin{cases} \dfrac{dn}{dt} = r\left(1 - \dfrac{n}{a}\right)^{\beta} + \begin{cases} bt, & t \le \theta \\ b\theta, & t > \theta \end{cases} \\ n(0) = 0. \end{cases} \quad (9)$$

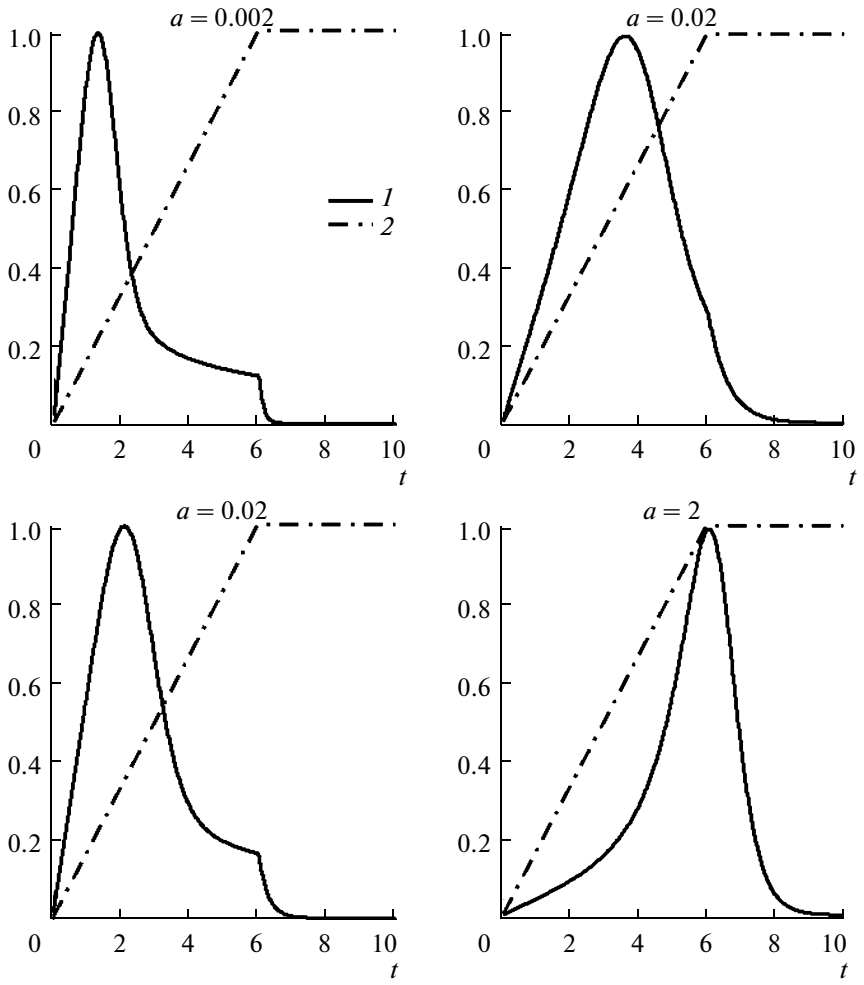

Fig. 24. Solutions of equation (9) (with the low rate of the "step" growth) for different a: (*1*) $1 - \frac{dn}{dt}$ from (9), (*2*) initiating step $f(t)$.

Equation (9) was solved numerically for different rates b of the increase in the function $f(t)$. β was taken to be 2, although the results will remain principally the same also with lower values.

With small rates of increase of $f(t)$, the activity dn/dt is swarm-like, and the maximum activity is determined by the capacity of the reservoir a (and, correspondingly, by the acting stresses). The peak activity shifts to the later times with increasing a; i.e., the delay of the commencement of the relaxation increases with the growth of a (Fig. 24).

The pattern of the dependence of the peak activity delay relative to the beginning of the step $f(t)$ on the stresses intensity may be inferred from the following considerations. It follows from equation (5) that a is equal to the total number of events: with $t \longrightarrow \infty$ reaches n is a stationary point of (5): a (a with $n = a = 0$). The experiments show that the total number of events a in each series may be approximated by the exponential dependence on the acting stresses (Figs. 3, 6, 11c, 17]. Consequently, we may assume that $a \propto \exp(\sigma)$. Thus, when studying the dependence of the solution to equation (9) on stresses, we should use the logarithmic stresses $\ln a$. The dependence of the maximum activity delay relative to the beginning of the load step on $\ln a$ is depicted in Fig. 25. This figure demonstrates also the examples of the dependences derived from the experiment. It is seen that the model curve is similar to its experimental dependences.

At the high rates of the increase of the step $f(t)$, the activity is characterized by the aftershock patterns, the delay in the beginning of the power-law decay of the activity increases with increasing a and, correspondingly, with increasing acting stresses (Fig. 26).

Thus, the results of mathematical modeling are qualitatively consistent with the laboratory data, which confirms, in our opinion, the validity of the idea of the competition between excitation and relaxation suggested for explaining the peculiarities in the development of failure during the transient mode of activity.

The considered mathematical model is schematic and requires further specification, primarily with the

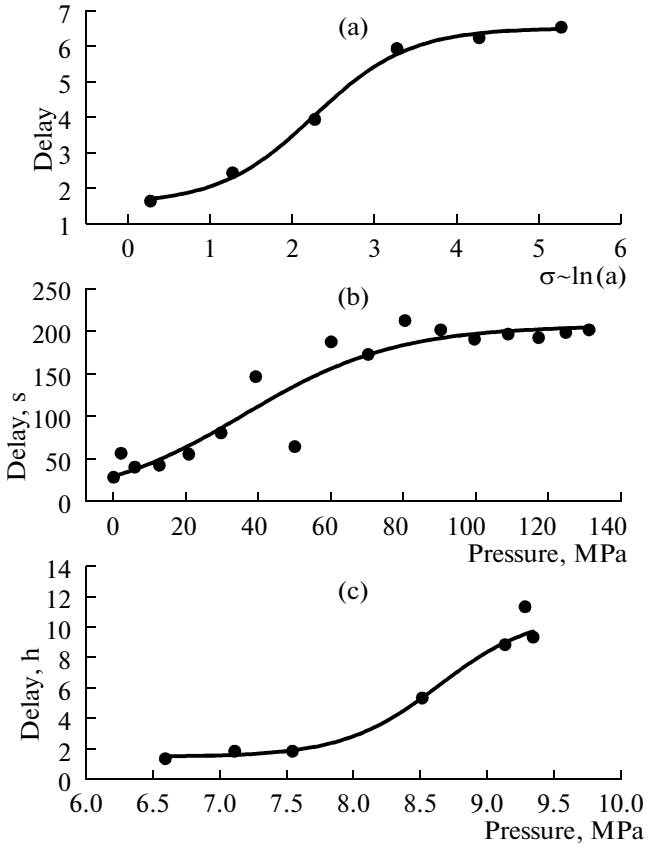

Fig. 25. Dependence of the delay in the commencement of relaxation on the acting stresses; (a) mathematical model, (b) laboratory experiment, (c) natural experiment in Soultz-sous-Forêts.

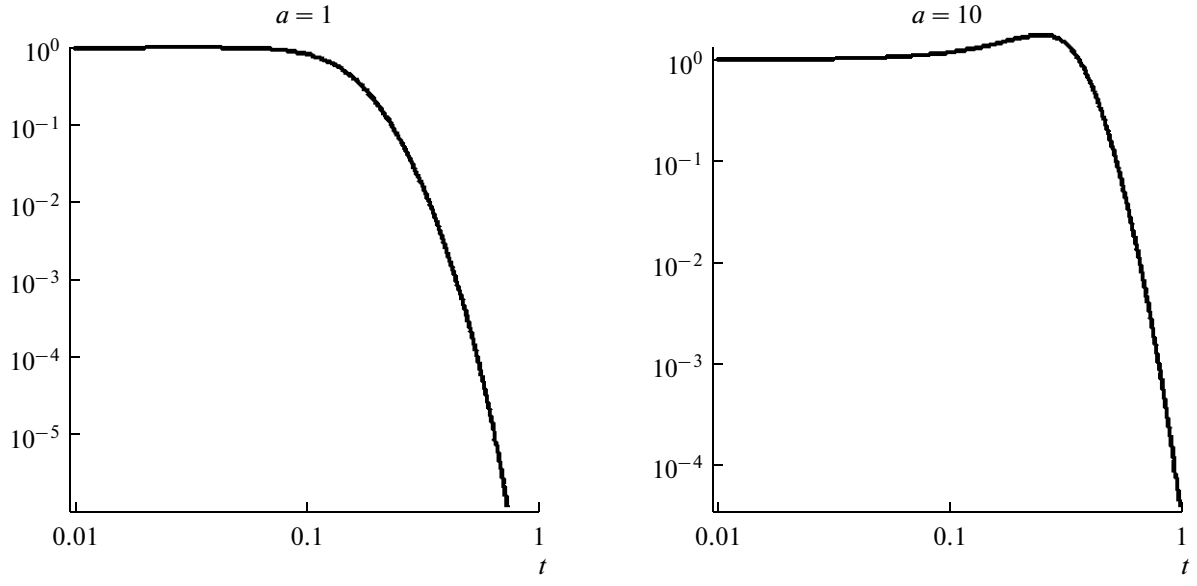

Fig. 26. Solutions of equation (9) (with the high rate of the "step" growth) for different a (the step of initiation at $t = 5 \cdot 10^{-4}$ is not shown).

account of different-scale failure and its temporal and spatial development. Therefore, in the present work we do not provide a thorough analysis of equation (9); we only demonstrate its main properties.

CONCLUSIONS

(1) Initiation of the rock fracturing by the stepped impact induces the transient acoustic–emission or seismic events, qualitatively similar to aftershocks and swarms. The rapid growth in the load generates the acoustic/seismic regime similar to the aftershock sequence, while the gradual increase induces swarm-like activity.

(2) The parameters of the induced activity change in a regular manner with increasing acting stresses: the stronger the stresses, the later the activity starts to decay; the parameters of Omori's law and the slope of the frequency-magnitude curve increase.

(3) Excitation and relaxation of the acoustic/seismic activity are reflected in the characteristic temporal change in the slope of the frequency-magnitude curve: the slope decreases at the stage of increasing activity and increases at the stage of decay, which indicates the transition of the failure from lower to higher levels (the crack instability avalanche scenario) and from higher to lower levels (the scenario of aftershocks) at the stages of the increase and decay, respectively.

(4) The model of the dynamics of the transient mode of activity induced by the external impact, which is based on the idea of competition between excitation and relaxation of the failure, explains qualitatively the main regularities identified in the laboratory and natural experiments.

(5) The revealed peculiarities in the initiation and development of the failure proved similar for the swarm and aftershock modes; there is also some analogy with the processes of the preparation of earthquakes. This observation provides the opportunity for considering different modes of seismic activity as the implementations of the same physical processes of the nucleation and development of the failure in different conditions. It is possible that in natural conditions, the impacts of natural factors (for example, local growth of deformations) may result in both the initiation of transient modes including swarms, and the occurrence of earthquakes, depending on the type of excitation, the properties, and the state of the geophysical medium.

ACKNOWLEDGMENTS

We are grateful to G.A. Sobolev for his fruitful discussions of the results and his useful recommendations. This work is supported by the Russian Foundation for Basic Research (project nos. 08-05-00248-a and 09-05-91056-NTsNI_a) and was carried out in the scope of scientific cooperation between the Institute of Physics of the Earth (Russian Academy of Sciences) and Institute de Physique du Globe de Paris.

REFERENCES

1. K. Aki, "Probabilistic Synthesis of Precursory Phenomena in Earthquake Prediction," Amer. Gephys. Union. An International Review, 556–574 (1981).
2. P. Audigane, J.-J. Royer, and H. Kaieda, "Permeability Characterization of the Soultz and Ogachi Large-scale Reservoir Using Induced Microseismicity," Geophysics **67**, 2004-211 (2002).
3. M. R. Ayling, P. G. Meredith, and S. Murrell, "Microcracking during Triaxial Deformation of Porous Rocks Monitored by Changes in Rock Physical Properties, I. Elastic-wave Propagation Measurements on Dry Rocks," Tectonophysics **245**, 205–221 (1994).
4. P. Bak et al., "Unified Scaling Law for Earthquakes," Phys. Rev. Lett. **88** (17). DOI: 10.1103/PhysRevLett.88.178501.
5. P. Bird, "An Updated Digital Model of Plate Boundaries," Geochemistry, Geophysics, Geosystems **4** (2). 1027, DOI: 10.1029/23001 GC 000252.
6. S. Bourouis and P. Bernard, "Evidence for Couplet Seismic and Aseismic Fault Slip during Water Injection in the Geothermal Site of Soultz (France), and Implication for Seismogenic Transients," Geophys. I. Int. **169**, 723–732 (2007).
7. T. T. Cladouhos and R. Marrett, "Are Faults Grows and Linkage Models Consistent with Power-low Distributions of Fault Lengths?" J. Struct. Geol. **18**, 281–293 (1996).
8. F. H. Cornet, "Comment on "Large-scale in situ Permeability Tensor of Rocks from Induced Microseismicity" by S. A. Shapiro, P. Augidane, J.-J. Royer," Geophys. J. Int. **140**, 465–469 (2000).
9. F. H. Cornet et al., "Seismic and Aseismic Slips Induced by Large-scale Fluid Injections," Pure Appl. Geophys. **10**, 563–583 (1997).
10. A. Corral, "Renormalization-group Transformations and Correlations of Seismicity" Phys. Rev. Lett. **95** (2005). DOI: 10.1103/PhysRevLett.95.028501.
11. A. J. DiGiovanni, T. Fredrich, D. J. Holcomb, and W.A. Olsson, "Micromechanics of Compaction in an Analogue Reservoir Sandstone, in *Proceedings of the North American Rock Mechanics Symposium, July 31, 2000*, Ed. by J. Girard et al., (2000), pp. 1153–1158.
12. *Earthquakes: Radiated Energy and the Physics of Faulting*, Ed. by R. Abercrombie et al. AGU Geophysical Monograph (2000).
13. K. F. Evans et al., "Microseismicity and Permeability Enhancement of Hydrogeologic Structures during Massive Fluid Injections into Granite at 3 km Depth at the Soultz HDR Site, Geoph. J. Int. **160**, 388–412 (2005a).
14. K. F. Evans, "Permeability Creation and Damage due to Massive Fluid Injections into Granite at 3.5 km at Soultz: 1. Borehole Observation," J. Geoph. Res. **110**, B04203 (2005b). doi: 10.1029/2004JB003168.
15. K. F. Evans, "Permeability Creation and Damage due to Massive Fluid Injections into Granite at 3.5 km at Soultz: 1. Critical Stress and Fracture Strength," J. Geoph. Res. **110**, B04203, (2005). doi: 10.1029/2004JB003168.
16. J. Fortin, S. Stanchits, G. Dresen, and Y. Gue'guen, "Acoustic Emission and Velocities Associated with the Formation of Compaction Bands in Sandstone," J. Geo-

phys. Res. **111**, B10203 (2006). doi: 10.1029/2005JB003854,

17. A. Gerard et al., "The Deep EGS (Enhanced Geothermal System) Project at Soultz-sous-Forêts (Alsace, France)," Geothermics **35**, 473–483 (2006).
18. G. S. Golitsyn, "Size distribution of the number of lithospheric plates , Physics of the Earth, No. 3, (2008).
19. K. Goto and K. Otsuki, "Size and Spatial Distributions of Fault Populations: Empirically Synthesized Evolution Laws for the Fractal Geometries," Geoph. Res. Lett. **31** (2004) L05601, doi: 10.1029/2003GL018868.
20. S. S. Grigoryan, "On the mechanism of Earthquake Initiation and Meaning of Empirical Regularities in Seismology," Dokl. Akad. Nauk SSSR **299** (5), (1988).
21. D. J. Hart and H. F. Wang, "Laboratory Measurements of a Complete Set of Poroelastic Moduli for Berea Sandstone and Indian Limestone," J. Geoph. Res. **100**, 17741–17751 (1995).
22. D. P. Hill, "A Model for Earthquake Swarms," J. Geoph. Res. **82**, 1347–1352 (1977).
23. T. Hirata, "Omori's Power Law Aftershock Sequences of Microfracturing in Rock Fracture Experiment," J. Geoph. Res. **92**, 6215–6221 (1987).
24. Li Hong, Li Shiyu, Xu Zhengyu, and Yin Xiangchu, "Experiment on Fracture Confining Pressure," Acta Seismologica Sinica **5**, 891–895 (1992).
25. Li Hong, Yin Xiangchu, Li Shiyu, and Li Jihan, "The Experimental Research on b-vale of AE for the Rock Specimens with Pre-existing Crack or Notch under Uniaxial Compression," Acta Seismologica Sinica **5**, 867–875 (1992).
26. H. Kawakata and M. Shimada, "Theoretical Approach to Dependence of Crack Growth Mechanism on Confining Pressure," Earth Planets Space **52**, 315–320 (2000).
27. G. King, "The Accommodation of Large Strain in the Upper Lithosphere of the Earth and Other Solids by Self-similar Fault System: The Geometrical Origin of b-value," Pure Appl. Geophys. **121**, 761–815 (1983).
28. A. V. Kol'tsov et al., "The Study of Destruction Preparation and Development in Rock Samples by the Geophysical Methods," Acta Geophysica Polonica **32**, 238–298 (1984).
29. B. V. Kostrov and Sh. Das, *Principles of Earthquake Source Mechanisms* (Cambridge Univ. Press, Cambridge, 1988).
30. V. S. Kuksenko, "Model of Transition from Micro- to Macrofracturing in Solid Bodies," in *Reports on the 1st All-Union Seminar "Physics of Strength and Plasticity* (Nauka, Leningrad, 1986. pp. 36–41 [in Russian].
31. A. V. Lavrov, V. L. Shkuratnik, and Yu. L. Filimonov, *Acoustic–Emission Memory Effect in Rocks* (MGU, Moscow, 2004) [in Russian].
32. X. Lei, O. Nishizawa, K. Kusunose, and T. Satoh, "Fractal Structure of the Hypocenter Distributions and Focal Mechanism Solutions of Acoustic Emission in Two Granites of Different Grain Sizes," J. Phys. Earth **40**, 617–634 (1992).
33. X. Lei, K. Kususnose, M. V. M. S. Rao, O. Nishizawa, and T. Stoh, "Quasi-static Fault Growth and Cracking in Homogenous Brittle Rock under Triaxial Compression Using Acoustic Emission Monitoring," J. Geophys. Res. **105**, 6127–6139 (2000).
34. D. A. Lockner, "The Role of Acoustic Emission in the Study of Rock Fracture," Int. J. Rock Mech. Min. Sci. Geomech. Abstr. **30**, 883–399 (1993).
35. D. A. Lockner and S. A. Stanchitts, "Undrained Poroelastic Response of Sandstones to Deviatoric Stress Change," J. Geophys. Res **107(B12)**, (2002). 2553, doi: 10.1029/2001JB001460.
36. D. A. Lockner, D. E. Moore, and Z. Reches, "Microcrack Interaction Leading to Shear Fracture," in *Proc. Thirty-third U.S. Symp. Rock. Mech.* (1992), pp. 807–816.
37. D. A. Lockner et al., "Quasi-static Fault Growth and Shear Fracture Energy in Granite," Nature **50**, 39–42 (1991).
38. D. A. Lockner et al., "Observations of Quasistatic Fault Growth from Acoustic Emissions," in *Fault Mechanics and Transport Properties of Rocks,* Ed. by B. Evans and T.-F. Wong (Academic Press, London, 1992), pp. 3–31.
39. A. V. Lyusina and V. B. Smirnov, "Temporal Grouping of Aftershock Sequences (Exemplified by Koalinga and Idaho Earthquakes on May 2, 1983 and October 28, 1983, Respectively)," Physics of the Earth, No. 8, 9–14 (1993).
40. I. G. Main, P. G. Meredith, and S. Jones, "A Reinterpretation of the Precursory Seismic b-value Anomaly from Fracture Mechanics," Geophys. J. **96**, 131–138 (1989).
41. G. G. Malinetskii and A. B. Potapov, *Actual Problems in Nonlinear Dynamics* (URSS, Moscow, 2002) [in Russian].
42. A. I. Malyshev and I. N. Tikhonov, "Nonlinear regular features in the development of the seismic process in time," Physics of the Earth, No. 6, 37–51 (2007).
43. D. Marsan and C. J. Bean, "Seismicity Response to Stress Perturbations, Analised for a Worldwide Catalogue," Geophys. J. Int. **154**, 179–195 (2003).
44. P. G. Meredith, I. G. Main, and C. Jones, "Temporal Variations in Seismicity during Quasi-static and Dynamic Rock Failure," Tectonophysics **175**, 249–268 (1990).
45. V. I. Mjachkin, W. F. Brace, G. A. Sobolev, and J. H. Dietrich, "Two Models for Earthquake Precursors," PAGEOPH **113** (1/2), 169–181 (1975a).
46. V. I. Mjachkin, B. V. Kostrov, G. A. Sobolev, and O. G. Shamina, "Basics of the Physics of the Source and Earthquake Precursors," in *Physics of the Earthquake Center* (Nauka, Moscow, 1975b, pp. 6–29 [in Russian].
47. D. Moore and D. Lockner, "The Role of Microcracking in Shear-fracture Propagation in Granite," J. Struct. Geol. **17**, 95–114 (1995).
48. C. Narteau, P. Shebalin, and M. Holschneider, "Temporal Limits of the Power Law Aftershock Decay Rate," J. Geophys. Res. **107(B12)** (2202). 2359, doi: 10.1029/2002JB001868.
49. A. Nicol et al., "Fault Size Distributions – Are They Really Power Law?" J. Struct. Geol. **18**, 191–197 (1996).
50. *NMSOP, IASPEI New Manual of Seismological Observatory Practice*, Ed. by P. Borman (GeoForschungZentrum, 2002).

51. M. S. Paterson and T. F. Wong, *Experimental Rock Deformation – The Brittle Field* (Springer, Berlin, 2005).

52. V. F. Pisarenko, *On the Law of Earthquake Recurrence* (Nauka, Moscow, 1975), pp. 6–29 [in Russian].

53. A. V. Ponomarev et al., "Physical Modeling of the Formation and Evolution of Seismically Active Fault Zones," Tectonophysics **277**, 57–81 (1997).

54. A. V. Ponomarev et al., "Seismic Parameters and Geophysical Variations before Zhangbei Earthquake," in *22th General Assembly of International Union of Geodesy and Geophysics, Abstracts* (Birmingham, 1999).

55. M. D. Read, M. R. Ayling, P. G. Mertedith, and S. Murrell, "Microcracking during Triaxial Deformation of Porous Rocks Monitored by Changes in Rock Physical Properties, II. Pore Volumometry and Acoustic Emission Measurements on Water-saturated Rocks," Tectonophysics **245**, 223–235 (1994).

56. Z. Reches and D. Lockner, "Nucleation and Growth of Faults in Brittle Rocks," J. Geophys. Res. **99**, 18159–18173 (1994).

57. V. R. Regel, A. I. Slutsker, and E. E. Tomashevskii, *Kinetic Nature of Strength of Solid Bodies* (Nauka, Moscow, 1974) [in Russian].

58. G. Yu. Riznichenko, *Mathematical Modeling in Biophysics and Ecology* (IKI, Moscow, 2003) [in Russia].

59. Yu. M. Romanovskii, N. V. N. V. Stepanova, and D. S. Chernavskii, *Mathematical Biophysics* (1984) [in Russian].

60. M. A. Sadovskii and V. F. Pisarenko, *Seismic Process and the Block Medium* (Nauka, Moscow, 1991) [in Russian].

61. M. A. Sadovskii, L. G. Bolkhovitinov, and V. F. Pisarenko, *Deformation of the Geophysical Medium and Seismic Process* (Nauka, Moscow, 1991) [in Russian].

62. A. A. Samarskii and A. P. Mikhailov, *Mathematical Modeling. Ideas. Methods. Examples*, (Fizmatlit, Moscow, 2005) [in Russian].

63. H. Scholz, *The Mechanics of Earthquakes and Faulting* (Cambridge Univ. Press, Cambridge, 2002).

64. A. A. Semerchan et al., "The Study of Precursors of Large Specimen Mechanical Fracturing," Dokl. Akad. Nauk SSSR **260**, 616–619 (1981).

65. S. A. Shapiro, P. Audigane, J.-J. Royer, "Large-scale in Situ Permeability Tensor of Rocks from Induced Microseismicity," Geoph. J. Int. **137**, 207–213 (1999).

66. S. A. Shapiro, P. Audigane, J.-J. Royer, "Reply to Comment by F.H. Cornet on 'Large-scale in Situ Permeability Tensor of Rocks from Induced Microseismicity," Geoph. J. Int. **140**, 470–473 (2000).

67. S. A. Shapiro, E. Huenges, and G. Born, "Estimating the Crust Permeability from Fluid-injection-induced Seismic Emission at the KTB Site," Geoph. J. Int. **131**, F15–F18 (1997).

68. M. Shimada and A. Cho, "Two Types of Brittle Fracture of Silicate Rocks under Confining Pressure and Their Implication in the Earth's Crust," Tectonophysics **175**, 221–235 (1990).

69. V. B. Smirnov, "The Assessment of Representativeness of Data on Earth Catalogues," Vulkalnol. Seismol., No. 4, 93–105 (1997a).

70. V. B. Smirnov, "Spatial and Temporal Variations in Parameters of Seismic Self-similarity," Vulkalnol. Seismol., No. 6, 31–41 (1997b).

71. V. B. Smirnov, "Assessment of the Duration of the Earth's Lithosphere Failure Cycle Based on Data from Earthquake Catalogues," Physics of the Earth, No. 10, 13–32 (2003).

72. V. B. Smirnov and V. D. Feofilaktov, "Fractal Properties of the Lithosphere Based on Code-waves of Local Earthquakes," Vulkanol. Seismol., No. 4, 52–56 (2000a).

73. V. B. Smirnov and V. D. Feofilaktov, "Fractal Properties of the Lithosphere Based on Code-waves of Local Earthquakes and Seismicity Structure in the Center of the Rachinskoe Earthquake," Vulkanol. Seismol., No. 6, 44–48 (2000b).

74. V. B. Smirnov and I. P. Gabsatarova, "Representativeness of the Earthquake Catalogue for the North Caucasus: Calculation Data and Statistical Estimates," Vestnik OGGGGN RAN, No. 4, 83–95 (2000).

75. V. B. Smirnov and A. V. Lyusina, "On Temporal Structure of Aftershock Sequences (Exemplified by the Alaska and Kamchatka Earthquakes)," Vulkanol. Seismol., No. 6, 45–54 (1990).

76. V. B. Smirnov and A. V. Ponomarev, "Regularities in Relaxation of the Seismic Regime according to Natural and Laboratory Data," Physics of the Earth, No. 10, 26–36 (2004).

77. V. B. Smirnov, A. V. Ponomarev, and A. D. Zav'yalov, "Peculiarities in the Formation and Evolution of the Acoustic Regime Structure in Rock Samples, Dokl. Akad. Nauk **343**, 818–823 (1995).

78. V. B. Smirnov, A. V. Ponomarev, and A. D. Zav'yalov, "The Structure of the Acoustic Regime in Rock Specimen and Seismic Process," Physics of the Earth, No. 1, 38–58 (1995).79.Smith W.D. The b-value As an Earthquake Precursor, Nature **289** (5794), 136–139 (1981).

80. G. A. Sobolev, *Basics of Earthquake Prediction* (Nauka, Moscow, 1993) [in Russian].

81. G. A. Sobolev and A. V. Ponomarev, "Acoustic Emission and Preparation Stages of Failure in the Laboratory Experiment," Vulkanol. Seismol., Nos. 4–5, 50–62 (1999).

82. G. A. Sobolev and A. V. Kol'tsov, *Large-scale Modeling of Earthquake Preparation and Precursors* (Nauka, Moscow, 1988) [in Russian].

83. G. A. Sobolev et al., "Precursors of the Failure in Water-containing Blocks of Rocks," Jour. Earthq. Prediction Res., No.1, 63–91 (1996).

84. D. Sornette and V. Pisarenko, "Fractal Plate Tectonics," Geoph. Res. Let. **30**, No. 3, 1105 (2003), doi:10.1029 / 2002GL015043.

85. Yu. M. Svirezhev, "Volterra and Recent Mathematical Biology," in *Afterword to the Book: "V. Volterra: Mathematical Theory of Struggle for Existence"* (Nauka, Moscow, 1976) [in Russian].

86. P. Tapponnier and W. F. Brace, "Development of Stress-induced Microcracks in Westerly Granite," Int. J. Rock Mech. Min. Sci. Geomech. Abstr. **13**, 103–112 (1976).

87. B. D. Thompson, R. P. Young R.P., and D. A. Lockner, "Fracture in Westerly Granite under AE Feedback and Constant Strain Rate Loading: Nucleation, Quasi-static Propagation, and the Transition to Unstable Fracture

Propagation," Pure Appl. Geophys. **163**, 995–1019 (2006). doi 10.1007/s00024–006–0054-x.

88. N. G. Tomilin, *Hierarchic Properties of Acoustic Emission under Rock Destruction* (FTI RAN, St. Petersburg, 1997) [in Russian].
89. D. Turcotte, *Fractals and Chaos in Geology and Geophysics*. Cambridge University Press, London, 1992).
90. M. Vogels, R. Zoeckler, D. M., Stasiw, and L.C., Cerny, "P. F. Verhulst's "notice sur la loi que la populations suit dans son accroissement" from correspondence mathematique et physique. Ghent, vol. X, London, 1838," J. Biol. Phys. **3** (4), 183–192 (1975).
91. J. Watterson, "Scaling Systematic of Fault Sizes on a Large-scale Range Fault Map," J. Struct. Geol. **18**, 199–214 (1996).
92. Lei Xinglin, K. Kusunose, T. Satoh, and O. Nishizawa, "The Hierarchical Rupture Process of a Fault: An Experimental Study, "Physics of the Earth and Planetary Interiors **137**, 213–228 (2003).
93. T. Yanagidani et al., "Localization of Dilatancy in Ohshima Granite under Constant Uniaxial Stress, J. Geophys. Res. **90**, 6840–6858 (1985).
94. G. Yielding, T. Needham, and H. Jones, "Sampling of Faults Populations using Sub-subsurface Data: A Review," J. Struct. Geol. **18**, 135–146 (1996).
95. H. Yukutake, "Fracture Nucleation Process in Intact Rocks," Tectonophysics **211**, 247–257 (1992).
96. A. Zang, F. C. Wagner, S. Stanchits, C. Janssen, and G. Dresen, "Fracture Process Zone in Granite," J. Geophys. Res., **105**, 23651–23661 (2000).
97. A. D. Zav'yalov, *Intermediate-term Prediction of Earthquakes: Basics, Methods, Realization* (Nauka, Moscow, 2006) [in Russian].
98. G. Zhang and Z. Fu, "Some features of Medium- and Short-term Anomalies before Great Earthquakes," in *Earthquakes Prediction. An International Review* (Amer. Geophys. Union. M. Ewing Ser., 1981), vol. 4, pp. 497–509.
99. J. Zhang J., T.-F. Wong, T. Yanagidani, and D. Davis, "Pressure-induced Microcracking and Grain Crushing in Berea and Boise Sandstones: Acoustic Emission and Quantitative Microscopy Measurements," Mechanics of Materials **9**, 1–15 (1990).
100. S. N. Zhurkov, "Kinetic Concept of Strength of Solid Bodies," Vestn. Akad. Nauk SSSR, No. 3, 46–52 (1968).
101. S. N. Zhurkov et al., "On Prediction of Rock Failure," Izv.AN SSSR. Fizika Zemli, No. 6, 11–18 (1977).
102. S. N. Zhurkov, V. S. Kuksenko, V. A. Petrov, et al., "Concentration Criterion of Volumetric Failure of Solid Bodies," in *Physical Processes in Earthquake Centers* (Nauka, Moscow, 1980), pp. 78–86 [in Russian].